A Coherent Treatment of QCD Radiation from Supersymmetric Quarks in the Antenna Shower Formalism

Ivan Begic

Supervised by
Assoc. Prof. Peter Skands

An Honours Thesis Presented for the Degree of
Bachelor of Science Advanced - Research (Honours)

School of Physics and Astronomy
Faculty of Science
Monash University
Australia

November 11, 2019

Abstract

In the phenomenology of high energy physics, Monte Carlo event generators are used extensively to simulate real-life particle collisions. Since analytical solutions of the Standard Model (SM), in particular Quantum Chromodynamics (QCD), are not known, various perturbative methods are implemented to simulate the complex quantum mechanics of fundamental particles at subatomic scales. This thesis presents two such models; the parton shower which is a monopole based treatment of QCD radiation, and the antenna shower which describes the radiation produced by dipoles of partons in a coherent manner. We apply the antenna shower to study the decay of a Supersymmetric top quark, a hypothetical Beyond the Standard Model (BSM) process. We make a comparitive study under a regime where all BSM masses are the same as their SM counterparts, and we find that the radiation pattern of a stop antenna is more sensitive to destructive interference than that of the top. Destructive interference effects begin to manifest beyond a $\sim 45^\circ$ emission angle of gluons from the (radiating) daughter of decay. This culminates in an extreme suppression where almost no radiation is emitted at 180°. Furthermore we compare the perturbative results underpinning the antenna shower to that of the parton shower, and observe that the latter amplitude begins to diverge from the former at an emission angle of $\sim 30^\circ$. Finally we investigate the radiation pattern in the context of shower evolution following an e^+e^- collision and observe that the angular distribution of gluon energies is everywhere smaller for the BSM process than the SM one, by an approximately constant amount for a large range of angles. We study as well the effect of the mass of a radiating particle on its collinear radiation properties, and observe suppression in agreement with the 'dead-cone' angle cited in the literature as roughly the mass/energy ratio of the radiating particle.

Acknowledgements

What a gruelling year this one has been. I could not have made it through without the help of some wonderful people.

First and foremost I cannot thank my supervisor Peter Skands enough for his wonderful guidance and infinite patience, through which I have learnt a tremendous amount of fascinating physics. Somehow he has helped me go from knowing a tiny amount of QFT and no particle physics to doing QCD research and writing what, I quite terribly hope, is at least a half decent thesis. Peter's enthusiasm and energy have inspired me to work harder and his high standards have really pushed me towards becoming a better physicist and careful scientist.

Secondly I must thank Helen Brooks for not only helping me with many physics and coding problems I got stuck on, but also for her compassion and efforts in caring for the Honours cohort. Having heard of the Spartan conditions of the coursework semester, Helen took the time to talk to the students, understand the shortcomings of the program itself, and take real and immediate action to try to improve it. Hopefully some of the changes implemented as a result of her efforts will give 2020's Honours cohort a better chance at staying afloat.

To that end, the late nights and mornings spent in New Horizons would have been a lot less fun, particularly these past few days, without the company of the fantastic cohort. Breaking up the tenuous writing with some smashing banter, and general disbelief that it is all drawing to an end, has made this past week more of a joy than I might have expected. A big round of thanks to everyone in the cohort, and a round of applause to all for reaching the finish line.

Finally I must thank my family for their support throughout this year. Honours has been a significant challenge, and getting to break the unending cycle of work with a dinner or two at home certainly helped me remember about the rest of life, when everything seemed like it was being swallowed up by physics. I am very grateful for all the help they have given me.

Contents

Chapter 1

Introduction

Experimental studies of particle collisions dating back to the 1970s [1, 2] have shown that in the collision of two subatomic particles, the resultant state is often one of high particle multiplicity, typically in highly collimated sprays of particles, known as jets. A good example is the decay of the W boson through the so called hadronic channel, where in the base process the W decays into a quark-antiquark pair, which later form composite particles known as hadrons. Before hadronization however, the quarks may undergo Quantum Chromodynamic (QCD) bremsstrahlung radiation by emitting gluons which in turn radiate may themselves, ultimately giving rise to a large number of final state particles, as shown in Figures 1.1 and 1.2. In particular, the trajectories have been reconstructed as the red, green, blue, black/yellow lines, demonstrating the highly collinear nature of radiation.

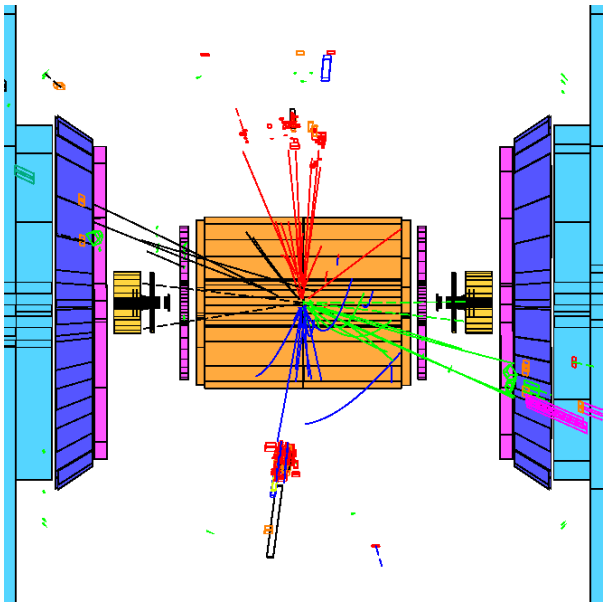

Figure 1.1: An $e^+e^- \to W^+W^- \to q\bar{q}q'\bar{q}'$ event from the second phase of the Large Electron Positron collider (LEP) in the OPAL experiment at 160 GeV center-of-mass energy. Figure courtesy of the High Energy Physics group at the University College London [3].

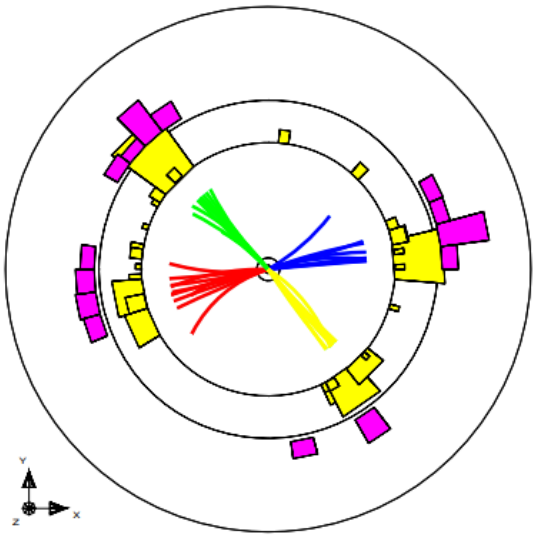

Figure 1.2: The same type of process observed with the OPAL detector, as seen projected onto the plane of the detector. Notably, the size of the pink boxes is proportional to the amount of energy due to hadronized particles in each jet. The yellow boxes similarly denote electromagnetic energies. Figure reproduced from Ref. [4].

Of particular importance to these events is that two particles have come in and n particles have come out. It is one of the principal efforts of QCD theory to simulate such events and predict experimental observables. One such approach is to calculate, to some k^{th} of perturbation theory, the matrix elements for the $2 \to 2$ event with all radiative corrections allowed up to order k. While successful in producing some broad features of showers such as angular distributions of jets and in particular for precise calculations of strong coupling, this approach is unable to precisely predict a number of interesting observables. For example fixed order attempts to describe the substructure of a jet have been unsuccessful [5, 6], however our understanding of jet substructure will only grow more important as calorimeters in detectors become more sensitive and are able to resolve finer details [7] in events.

It was found in the 1970s, however, that using the parton model[1] of Bjorken and Feynman [8, 9], a 'parton shower' framework provided a very versatile method of predicting experimental outcomes. The papers of, in particular, Dokshitzer, Gribov, Lipatov, Altarelli and Parisi [10–13] prompted the development of the parton shower formalism, and implementations into Monte Carlo event generators quickly met success in describing a host of experimental phenomena [4, 6, 14], including, for example, the substructure of jets.

The essence of the shower method is the following: instead of calculating quantum field theory (QFT) amplitudes exactly to a given order, one approximates the amplitude for a single emission in a region where it is most enhanced, i.e. where the amplitude becomes singular. Analytically one finds that enhancements may come from low energy (soft) emission, or, as indicated in the Figures above, collinear emission. Traditional parton shower models implement precisely the amplitudes derived in the latter case. In this way, the shower implements an approximate result that, due to the universality we will discuss in the next section, resums the perturbative expansion to recover higher order information through a Markov chain of recursive radiative corrections.

A problem of this method is precisely that these probabilities are accurate only in the collinear limits. This works well when, as in Figure 1.2, the event is sufficiently soft that collinear jets dominate the event, i.e. one may observe the pink and yellow boxes not due to the resolved jets. However, due to the scaling properties of QCD [15], if for instance the collision energy of some event is scaled by a factor of 10, the original rate of X GeV jet production will match (approximately) the rate of $10X$ GeV jet production in the harder event. An immediate consequence is that soft corrections become more prominent in higher energy collisions, which is certainly the direction that modern colliders are tending to in the search for physics Beyond the Standard Model (BSM). While there are methods of recovering soft radiation effects, it is nonetheless clear that more accurate treatments of radiation are desirable for simulations of collider physics.

The most commonly used event generators on the market are Pythia, Sherpa, and Herwig [14]. Each of these generators aims to simulate the same physics, albeit in slightly different ways. Most recently in 2016 [16] the Vincia plugin to Pythia8 was developed and implemented as a generalization of the parton shower; the antenna, or dipole-antenna shower. This method, first implemented by Gustafson and Pettersson [17] in 1988, based on their earlier theoretical work [18] and that of Azimov, Dokshitzer, Khoze and Troyan [19] in 1986 and 1985 respectively, consists in evolving a shower of dipoles rather than individual partons, whereby iterative gluon emission can be described in a pairwise manner between two colour-connected quarks, i.e. in a chain of $2 \to 3$ parton

[1] wherein the constituent parts of a hadron, namely quarks and gluons, are referred to collectively as partons

emissions, as opposed to the $1 \to 2$ parton emissions of the traditional shower. While the parton shower is in some ways a semi-classical process, the antenna shower captures essential quantum interference effects, in particular due to dipoles of colour charges radiating gluons coherently (but not of any higher multipoles). In this way the parton shower is a limiting case of the antenna shower.

In this work, we study the extention of the antenna formalism to a hypothetical New-Physics process predicted by supersymmetric extensions to the Standard Model. We observe interesting differences to the corresponding Standard Model process and make attempts to physically understand them. The thesis is structured as follows. We will begin with a very brief overview QCD as a QFT, and establish the background physics involved in the event generators that are of interest. We will briefly introduce our case study of spin-0 colour-triplets, before turning to the derivation of the antenna function in Chapter 3, and discussing the implementation of the kinematics and phase space. In Chapters 4 and 5.1 we will briefly describe the implementation in Vincia and present our findings.

Chapter 2

Background Theory

2.1 Quantum Chromodynamics

We begin by establishing some orientation on the basic properties of QCD [15]. First and foremost, QCD is a theory of the strong interaction which is responsible for the strong nuclear force. At large scales it is what provides the binding energy for protons and neutrons to form nuclei, and at small scales describes the fundamental fermions, called quarks, which are the only (known) fermions that undergo strong interactions. The quarks come in six flavours; up, down, charm, strange, top and bottom. The up-type quarks (up, charm, strange) have electric charge 2/3 and the down-type quarks (down, strange, bottom) have electric charge $-1/3$, in units of fundamental charge. The quarks experience the electromagnetic force due to their electric charges, which are mediated by photons, but they also possess a 'colour' charge; red, green, or blue; and this is what allows them to undergo strong interactions, which are mediated by gluons.[1]

2.1.1 Lagrangian

While quantum electrodynamics (QED) is a $U(1)$ gauge theory, meaning that the fields in question entertain a local $U(1)$ gauge symmetry $e^{i\lambda(x)}$, QCD is an $SU(3)$ gauge theory. The structure of the Lagrangians of both theories is essentially the same, however due to the extra structure granted by $SU(3)$, QCD possesses a much richer dynamical structure. It is simplest to understand QCD starting with the QED Lagrangian, whose details we refer the reader to [20] for. Using $\hbar = c = 1$, the Lagrangian of electrodynamics is

$$\mathcal{L}_{\text{QED}} = -\frac{1}{4} F_{\mu\nu} F^{\mu\nu} + \bar{\psi} \left(i\gamma^{\mu} D_{\mu} - m \right) \psi \tag{2.1.1}$$

with the field strength tensor $F_{\mu\nu} = \partial_{\mu} A_{\nu} - \partial_{\nu} A_{\mu}$, the covariant derivative $D_{\mu} = \partial_{\mu} + ieA_{\mu}$, and where, denoting an anticommutator by $\{\cdot, \cdot\}$, the set of four, 4×4, γ matrices satisfy the Clifford algebra $\{\gamma_{\mu}, \gamma_{\nu}\} = 2\eta_{\mu\nu}$. The e at this stage can simply be thought of as the coupling constant, defining the strength of interactions between charged fermions and the photon field, however as we will see in the next section this is not quite the full story. The above Lagrangian describes how a spin-1/2 field couples to a spin-1 field under a local $U(1)$ gauge symmetry.

The generalization to $SU(3)$ simply entails replacing the covariant derivative with a coloured covariant derivative. We will simply state without much justification (however a brief review of

[1] It is worth noting that force carriers such as gluons and photons are known as gauge bosons because they are integer spin particles and have a 1:1 correspondence with the generators of the gauge symmetry group [20]

Lie group theory is provided in Appendix F), that an $SU(3)$ gauge transformation is of the form $\psi \to \exp\left(it^a_{ij}\lambda^a\right)\psi$ for t^a being the generators[2] of $SU(3)$, $a \in 1, 2..., 8$, $i, j \in 1, 2, 3$. The i and j are the colour indices for the quarks, and the a is a colour index for the gluons, known as the adjoint index. The matrices t^a_{ij} define the colours of the quarks that a given gluon can couple together. Enforcing local gauge symmetry requires us to redefine the covariant derivative analogously as

$$(D^\mu)_{ij} = \delta_{ij}\partial_\mu + ig_s t^a_{ij} A^\mu_a \tag{2.1.2}$$

where g_s is the strong coupling $g_s^2 = 4\pi\alpha_s$. The fields A^μ_a are now the gluon fields and we define the gluon field strength tensors as

$$G^a_{\mu\nu} = \partial_\mu A^a_\nu - \partial_\nu A^a_\mu + g_s f^{abc} A^b_\mu A^c_\mu \tag{2.1.3}$$

where f^{abc} are the structure constants[3] of $SU(3)$. Finally, since we now have 3×3 matrices in the Lagrangians, the fields that they couple to must be triplet fields, namely what was originally simply ψ in electrodynamics becomes $\psi_i = \psi c_i$ where c_i is a vector in colour space. The addition of the structure constants in (2.1.3) reflects the non-Abelian nature of $SU(3)$, namely that elements of this group do not commute. The immediate consequence of will be seen once we write down the full QCD Lagrangian [15] for quarks q of mass m_q and colours i, j as

$$\mathcal{L}_{\text{QCD}} = -\frac{1}{4}G^{\mu\nu}_a G^a_{\mu\nu} + \bar{\psi}^q_i\left(i\gamma^\mu\left(\delta_{ij}\partial_\mu + ig_s t^a_{ij}A^a_\mu\right) - m_q\right)\psi^q_j \tag{2.1.4}$$

where the sum over q, i and j is implicit. Observing this Lagrangian, we see that the $G^a_{\mu\nu}$ terms give rise to gluon-gluon interactions, of which there is no analogue in QED. As noted above, we have quark-quark interactions via the gluons through $t^a A^a$, and we see from squaring $G^a_{\mu\nu}$ that there is a three-gluon vertex of order α_s, and a four-gluon vertex of order α_s^2.

2.1.2 Running Coupling

It is a famously known property of renormalizable gauge theories [15, 21] that the coupling constants are not truly constants, but have a dependence on the energy scale of the process being studied. We will make a very brief description here of this phenomenon. The coupling can either increase or decrease with the energy scale Q, and it does so logarithmically according to the famous β function, where $\partial\alpha_s/\partial \ln Q^2 = \beta(\alpha_s)$. In particular we have, to leading order in α_s [15, 22], that $\beta \propto -11N_C + 2n_f$. For QCD, having $N_C = 3$ colours and $n_f = 6$ fermions, $\beta < 0$: the coupling weakens logarithmically with the energy scale. For this monumental discovery, Gross, Politzer and Wilczek were awarded the Nobel prize in 2004.

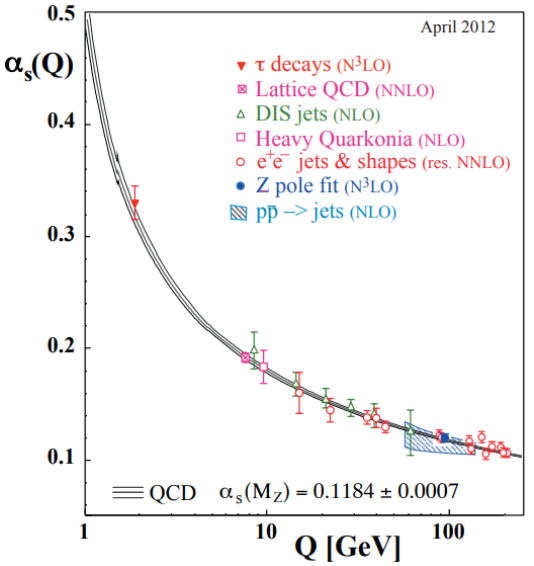

Figure 2.1: Numerical and experimental determinations of the strong coupling at higher energy scales. Figure taken from [15].

[2] See the appendix for a definition
[3] See the appendix for a definition

We refer the reader to a number of good introductions to renormalization [15, 21, 23, 24], however of primary relevance to us, we show in Figure 2.1 a number of measurements of α_s as a function of the energy scale probed. The running of the coupling will eventually take it to a value beyond unity at some energy scale below 1 GeV. At this scale, there is no longer any suitable parameter to apply a perturbative expansion with in QCD, and alternative quantitative techniques must be applied to describe hadronization, whereby quarks and gluons interact to form the hadrons. The most successful of these is the Lund string model, however a discussion is beyond the scope of this thesis and we refer the reader to introductory texts and reviews as [14, 21]. As we will discuss shortly, the focus of this thesis will be on describing hard processes, namely those with $Q > 1$ GeV, using perturbation theory.

2.2 Overview of the Physics in a Collision

In a typical LHC collision one observes a vast range of energy scales. To name only two, the CMS and ALICE experiments at the LHC have studied pp collisions at up to 14 TeV, with some studies found in Refs. [25–27]. Accompanied with any processes such as this will be a large amount of bremsstrahlung radiation, likely spanning orders of magnitude in energy. Consequently, in such an experiment one will necessarily be probing a large amount of very complicated and scale-dependent physics. For a theoretical treatment it is necessary to implement the factorization theorem [14, 15], whereby each of the different 'components' of an event may be factored away from the rest, analyzed in isolation, and later combined to obtain the overall probabilities, cross sections, etc. that one may desire. The utility of this is that we may isolate our problem into the high energy regime where perturbative QFT can be applied.

As a particular case study relevant for this thesis, consider the collision of an electron positron pair as shown in Figure 2.2. Before discussing the QCD effects we may note in passing that prior to collision, the electron or positron may undergo QED bremsstrahlung (which has not been included in the Figure). This may give rise to photons which in turn may split into further e^+e^- pairs, and this already generates some multiplicity to the final state. However, since the strong coupling dominates the electromagnetic coupling at later stages of the shower,[4] we will turn our eye instead to the QCD radiation as a primary contributor to final state multiplicity and sole contributor of hadronic states. Continuing then, the annihilation may give rise to a quark-antiquark pair at some energy scale, or virtuality,[5] Q^2. These quarks may then undergo strong interactions themselves. Considering the $\bar{q}$ in the lower branch of Figure 2.2, it may propagate for some time before emitting a gluon. This gluon may then propagate itself and either emit further gluons and split into $q\bar{q}$ pairs, as in the second emission, or continue without any further radiation. In this way the shower will develop until the virtualities of the daughter partons reach some scale Q_0^2 sufficiently small so that $\alpha_s \sim 1$, leading to the combination of partons into the colourless final state hadrons that are observed at the detector.

Similar phenomena occur in the hadron-hadron collisions at the LHC, however the complexity of such events is vastly greater than for electron-positron collisions. Not only do the incoming particles now have the option to undergo QCD radiation, but when the very energetic hadrons collide, it will be the constituent partons within them that collide. This offers the possibility of having more than one pair of partons colliding, possibly with several different collision energies, depending

[4] The β function of electrodynamics carries the opposite sign, so that while α_{QCD} grows, α_{QED} weakens.

[5] We define virtuality as a measure of how off-shell a particle is, with the on-shell condition for a mass m particle being that its 4-momentum p satisfies $p^2 = m^2 = E^2 - \vec{p}^2$

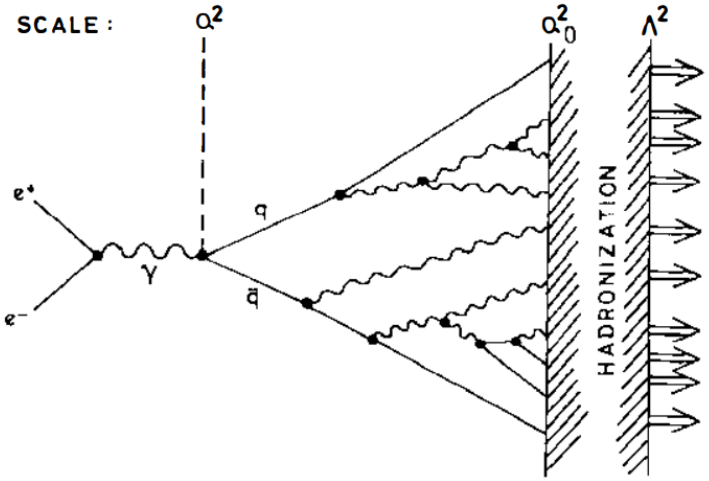

Figure 2.2: A schematic illustration of an electron-positron collision, producing a virtual photon which splits into a quark-antiquark pair that then undergo bremsstrahlung radiation before hadronizing. One may consider the vertical axis as space, the horizontal axis as time. Figure reproduced from Ref. [6].

on the probability distribution of finding partons of a given energy within the hadron. For our study, however we consider only e^+e^- collisions which in comparison are quite simple. The bulk of our analysis will consist in analyzing and improving the description of radiative corrections: for instance, how do the two gluons emitted between the $q\bar{q}$ pair interfere with one another, and how may we describe the evolution of such a process? To address these questions we therefore begin with an overview of traditional parton shower methods, before describing the antenna formalism.

2.3 Parton Showers

To set the stage we will first consider an attempt to describe the observed spectrum of particles through a fixed order perturbative treatment in QFT. For instance we may consider top decay through $e^+e^- \to t\bar{t} \to bW^+\bar{b}W^-$. A straightforward calculation of this amplitude, i.e. the Born level process, predicts only four particles in the final state. We may consider then a radiative correction, i.e. the Born+1 process. We know already from our discussion above that to accurately match experiment, we require many radiative corrections. Let us consider then the base case of one emitted gluon. We may start by calculating the squared matrix elements of order α_s^2. These will be the two diagrams in the leftmost column in Figure 2.3.
A full computation, however, reveals infrared (IR) divergences, namely that the square matrix elements are singular in the limits where the radiated gluon is either collinear to the parent, or infinitely soft. The problem of non-degenerate perturbation theory presents itself: from the point of view of measurement, one cannot distinguish between, for example, two exactly collinear gluons or one gluon with a virtual correction. So, in computing this amplitude, we must include as well the virtual corrections, such as the loop diagrams in Figure 2.3. The famous theorem of Kinoshita, Lee, Nauenberg [28, 29] proves that when we include all $\mathcal{O}(\alpha_s^2)$ processes that the divergences of the virtual corrections cancel exactly with those of the real corrections. In this way, quantum field theory preserves unitarity; one must simply sum over all possible events to obtain a meaningful probabilistic description of a splitting process. We note that, once all diagrams of a given order in the amplitude have been written, combining them to obtain the correct order in the squared

amplitudes is slightly subtle and discussed in detail in [15].

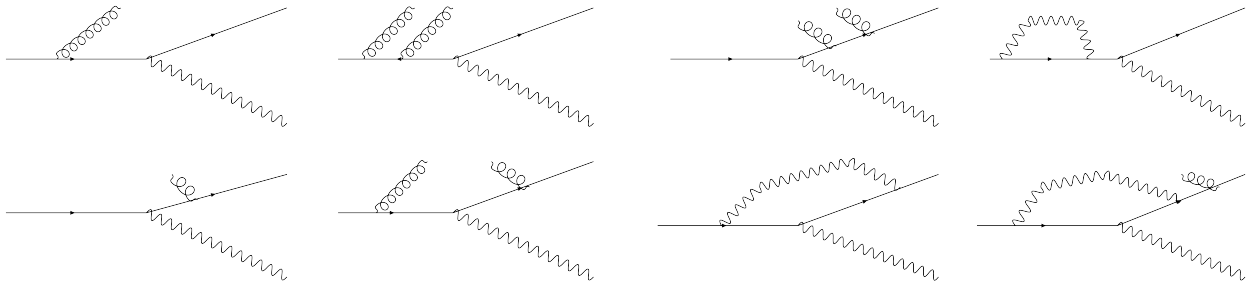

Figure 2.3: Some possible diagrams that contribute to radiative corrections of various orders, both real and virtual. The solid lines are quarks, the wave line is a W boson, and the looped lines are gluons.

Even with one emitted gluon the calculation is quite complicated, and for any hope at matching experiment we require more radiation, as per the remaining diagrams in Fig 2.3. At higher orders there are a large number of possibilities to consider: there may be more gluons emitted from the quarks, or the original gluon that was emitted will split into a quark and gluon pair, we may have further virtual corrections and even virtual corrections to the virtual corrections. Some of these have been shown in Fig. 2.3, however this is only a small subset of the all possible corrections that can occur.[6] It is quite clear then that any attempt to compute exactly with perturbation theory the detailed structure of an event is not realistically achievable. Much effort has been undertaken in recent years to obtain analytical expressions at higher orders. Next to Leading Order (NLO) computations have largely been automated, but calculations beyond this are still the subject of research in the fixed order QCD community [31].

What saves the day and offers us an alternative method is the universality of gauge theory amplitudes. Consider an emission of a gluon in some process [15], as shown in Fig. 2.4.

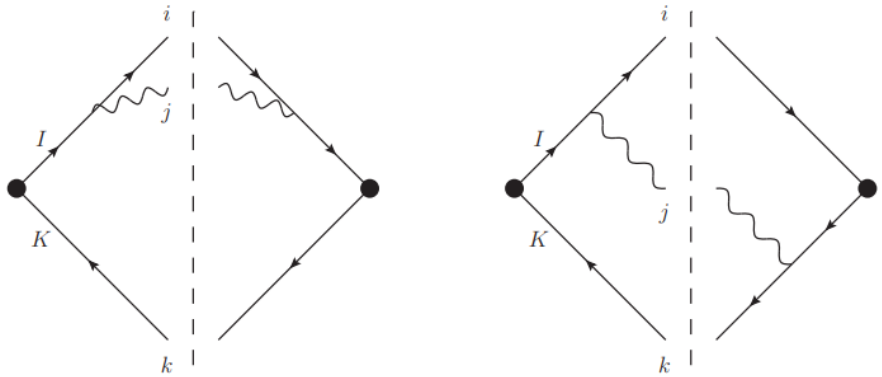

Figure 2.4: A pictorial representation of the squared matrix elements for a gluon emission, reprodued from Ref [15]. On the left is shown the squared matrix element for gluon emission off the I parton, and on the right is the inner product between gluon emission off the I and K partons, i.e. the interference diagram.

We know from the general structure of Feynman diagrams that the corresponding matrix ele-

[6] A more detailed treatment, displaying more of the higher order possibilities, can be found in [30]

ment has a propagator denominator of $p_I^2 = (p_i + p_j)^2 = 2p_i.p_j$ (assuming massless on-shell quarks). This will hold true whether this is the first or the n^{th} emission, and it follows then, that the amplitude (and its square) is singular when $p_i.p_j = 0$. Expanding this product gives $p_i.p_j = E_iE_j - |\vec{p_i}||\vec{p_j}|\cos(\theta_{ij}) = E_iE_j(1 - \cos(\theta_{ij}))$, so singularities occur for soft or collinear emissions, and corresponds to the propagator p_I coming on shell. Likewise, in the interference process we pick up propagators from both branchings to end up with a square amplitude containing $\sim p_i.p_k/(2p_i.p_j\ p_j.p_k)$, known as the soft eikonal factor. The singularities in this case correspond to I and K coming on shell, which can occur simultaneously if the gluon is soft. It is interesting to consider the *pole structure* of this amplitude. We can understand this by considering the squared amlitude with a phase space measure, in general something including a term

$$P\ \mathrm{d}\Phi \sim \left(\frac{p_i.p_k}{2p_i.p_j\ p_j.p_k} + \frac{p_i.p_j}{p_j.p_k}\right)\mathrm{d}\Phi \tag{2.3.1}$$

Now, in a small angle approximation the phase space (shown in Appendix A) may be written $\mathrm{d}\Phi \propto E_j\mathrm{d}E_j\mathrm{d}\theta_{jk}$. The above equation will then reduce, under the same approximations, to include terms of the form

$$P\ \mathrm{d}\Phi \sim \left(\frac{1}{E_j^2\theta_{jk}} + \frac{1}{E_j\theta_{jk}}\right)\ E_j\ \mathrm{d}E_j\ \mathrm{d}\theta_{jk} \tag{2.3.2}$$

Observe then that the net amplitude carries a first order pole for collinear radiation off either parton in the second term, and a second order pole for soft *and* collinear radiation in the first term. Upon integration of the antenna function the pole order corresponds to the power of logarithmic enhancements: either log for single poles and $\log^2$ terms for double poles. Thus the radiative corrections are logarithmic in each of the collinear or soft limits, and squared-logarithmic in the soft and collinear limit.

In this sense, the radiation from any stage of the shower follows a universal form, wherein the behaviour of any given branching is entirely local and only depends on the particles involved in that branching process. Furthermore each amplitude contains universal soft eikonal and collinear terms, capturing the leading singularities of the process. In a general sense, then, the singular parts of the correction amplitude factorize, with some function f that captures these singularities, as

$$|\mathcal{M}_{n+1}|^2\alpha\ f\ |\mathcal{M}_n|^2 \tag{2.3.3}$$

As we have mentioned, in the case of parton showers, the function f is evaluated in the collinear limits to give the DGLAP splitting kernel.

The parton shower algorithm, then, is based entirely on this principle: that our QCD amplitudes factorize in this universal way and exhibit soft and collinear singularities. In general, the analytical forms of the splitting kernels will contain some nonsingular, process-dependent terms, but these we will discuss more when we begin considering the antenna shower. Nonetheless at each and every stage of the splitting, there will exist a set of universal singular terms that dominate the shower evolution.

In this way, one may construct an algorithm whereby any given parton may branch off to whatever daughters are allowed to it by QCD, according to the probability described by this function f, and construct a shower of partons through an iterative Markov chain. We note here that the nature of the Markov chain is such that it automatically preserves unitarity, without the need to consider

NLO calculations; indeed we conclude this introduction by quoting the seminal paper of Alterelli and Parisi where such a language was introduced [13]:

> *In our opinion the present approach, although less general, is remarkably simpler than the usual one since all relevant results can be derived in a direct way from the basic vertices of QCD, with no loop calculations being involved.*

2.3.1 Parton splitting

We will now begin to describe the mathematics of parton showers in more detail. To begin with, consider one single branching process somewhere in a shower, where $a \to bc$. We call a the parent or mother parton and b and c the daughter partons. There are two possibilities, namely that the branching happens after the hard process, generating final state radiation, or that the branching happens before the hard process, generating initial state radiation. Since we study e^+e^- events where there is no initial state QCD radiation, we will restrict ourselves to the former case.

Let $z = E_b/E_a$ (i.e. the fraction of energy that the daughter takes of the mother) and Q^2 be some variable characterizing, for example, the virtuality, momentum exchange or transverse momentum of the branching, in units of GeV^2. The Q^2 is known as an evolution variable and is not unique, and several definitions may be implemented, even within a single shower. Each choice carries its own advantages and disadvantages, and we will discuss some of these in the next section. These evolution variables encode evolution in the sense that, in each consecutive branching, the parent partons have less and less energy to give to their daughters, and thus the Q^2 will tend to zero. Physically, the Q^2 may represent a sort of time in the shower: in final state radiation one evolves the shower from partons emitted at a maximum Q^2_{start}, typically equal to the energy scale of the hard process, down to the cutoff where hadronization takes over $Q^2_{\text{stop}} \sim 1$ GeV. Noting this and that the integration measure is proportional to a dQ^2/Q^2, it is convenient in discussing the evolution of a shower to define a variable $t = \ln(Q^2)$, as a kind of 'time.'
As mentioned in the introduction, the parton shower model is based on the collinear singularity of the amplitude factorization. Namely,

$$|\mathcal{M}_{n+1}|^2 \propto P_{a\to bc}(z)|\mathcal{M}_n|^2 \tag{2.3.4}$$

where $P(z)$ is known as the DGLAP splitting kernel for the process [10–13], the functional forms of which may be found in Appendix A. These splitting kernels are derived from the matrix elements by taking a small angle approximation between the daughter and parent partons. The proportionality constant carries a factor of the coupling g_s^2 and a colour factor to reproduce the correct statistics - this will be discussed in more detail in Chapter 3. The DGLAP kernels encode the probability that a radiative correction occurs, and so together with the appropriate branching phase space, the net differential probability of branching in some energy fraction range dz and 'time' dt is then [32]

$$d\mathcal{P}_a\ dt\ dz = d\mathcal{P}_a \frac{dQ^2}{Q^2} dz = \sum_{b,c} \frac{\alpha_s(t)}{2\pi} P_{a\to bc}(z)\ dt\ dz \tag{2.3.5}$$

Therefore the net branching probability in some time δt after t will be

$$\mathcal{I}_{a\to bc}\ \delta t = \int_{z_-(t)}^{z_+(t)} d\mathcal{P}_a\ dz\ \delta t \tag{2.3.6}$$

where we have allowed some upper and lower limits to the branching, for example to prevent profuse emission of infinitely soft gluons (which anyway a reasonable definition of the resolution measure t

would not allow to resolve). The summation of parton types b and c is now also done implicitly. It follows that the probability of *no* emission in this time is $(1 - \mathcal{I}_{a\to bc}\ \delta t)$. If evolving a parton shower, then, the probability that nothing happens between times t_0 and t (with $t < t_0$ in a final state evolution) is just the product of the probabilities that nothing happens between the incremental timesteps $(t_0, t_0 - \delta t)$, $(t_0 - \delta t, t_0 - 2\delta t)$ and so forth. Taking δt infinitesimal we have the Sudakov form factor

$$\Delta_a(t_0, t) := \mathcal{P}_{\text{no-emission}}(t_0, t) = \lim_{N\to\infty} \prod_{i=1}^{N} (1 - \mathcal{I}_{a\to bc}\delta t) = \exp\left(-\int_t^{t_0} dt'\ \mathcal{I}_{a\to bc}(t')\right) \tag{2.3.7}$$

which forms the basis of any shower algorithm. This in fact generalizes to the case where the splitting kernel, that is, the function f in Eq. (2.3.3), is not a DGLAP kernel but possibly some more general function. In either case, the Sudakov factor has a general form

$$\Delta_a(t_0, t) = \exp\left(-\int_t^{t_0} \mathrm{d}\Phi\ f\left[\Phi\right]\right) \tag{2.3.8}$$

where we have written $f[\Phi]$ to emphasize that there are a number of possible variables that one can choose to describe the phase space.

Using this picture, it is in principle a simple matter to implement the following algorithm to generate a shower, known as the Sudakov algorithm:

1. Start the shower at the time/energy scale t_0 corresponding to the hard process in question
2. Choose randomly some $\mathrm{R} \in [0, 1]$
3. Solve $R = \Delta_a(t_0, t_1)$ for t_1
4. Generate a splitting of a parton at time t_1
5. Repeat the process to generate further splittings
6. Iterate over all parton branches until the cut-off energy $Q^2_{\text{stop}} = t_{\text{stop}}$ has been reached

What is happening here is that we have some basic probability amplitudes that determine how likely it is for an event to occur, or more precisely; to not occur. So we can assume that something happens at some time t with some probability R and solve for that t. Then the shower branches and by universality each branch evolves in the same way. Over a large number of simulations, we build up a statistical distribution of events which in principle approximates quite well the true quantum mechanics of the process.
One may describe the overall Markov chain with a unitary operator [33] S that generates a recursive shower starting from n particles and evolving between some start and end times $t_{\text{start}}, t_{\text{end}}$:

$$\begin{aligned} S(\{p_n\}, t_{\text{start}}, t_{\text{end}}) &= \Delta\left(\{p_n\}, t_{\text{start}}, t_{\text{end}}\right) \\ &+ \sum_{\substack{\text{possible branchings} \\ IK\to ijk}} \left(\int_{t_{\text{start}}}^{t_{\text{stop}}} \mathrm{d}\Phi f[\phi]_{IK\to ijk} \left[\Delta\left(\{p_n\}, t_{\text{start}}, t_{\text{event}}\right) \times S\left(\{p_{n+1}\}, t^{\text{event}}_{\text{restart}}, t_{\text{stop}}\right)\right]\right) \end{aligned} \tag{2.3.9}$$

where in the first term we capture the events where nothing at all happens in the branching, and in the second term we have: a sum over all possible branchings that can occur, each taking the form

of; a no-emission evolution up to the event scale t_{event} (which has been solved for in the algorithm enumerated above); with probability according to the splitting function implemented, f; and then the operator is applied again to generate the next evolution, starting from the scale of the event and continuing to evolve forward to t_{stop}.

It is noteworthy that in a fixed order approach, preservation of unitarity was achieved in the relatively nontrivial manner of including all radiative corrections at a given order. In the parton shower approach, since we are preserving unitarity *by default* in the Markov chain, we not only have a working simulator of a complex quantum process, but we are also capturing through unitarity some of those higher order corrections despite only implementing tree-level splitting probabilities.

2.3.2 Sudakov Veto Algorithm

In general, the integrand of the Sudakov factor may be sufficiently complicated that inverting $R = \Delta_a(t_0, t)$ may be very computationally expensive. For this reason we implement the Sudakov Veto algorithm which is an elegant way to obtain the same solution with much less work [34].

Suppose that in some shower algorithm such as the one described above, we need to solve for t in

$$\ln R = -\int_t^{t_0} A(t')\ dt' \tag{2.3.10}$$

and that A is some very complicated function. The Sudakov veto algorithm consists in adding some positive definite term B to overestimate the integral:

$$\ln R = -\int_t^{t_0} A + B\ dt' \tag{2.3.11}$$

where B is chosen in a way to ensure that the integration is quite simple. Then one can solve for the value of t in an inexpensive manner and accept it with a probability

$$P_A = \frac{A}{A+B} \tag{2.3.12}$$

and reject it with a probability

$$P_B = \frac{B}{A+B} \tag{2.3.13}$$

We prove in Appendix B the surprising result that this algorithm reproduces exactly the same branching distribution as a solution of the true Sudakov factor would; namely that the overestimation of the branching probability due to B is compensated for in an exact way by only accepting branchings with a probability P_A.

2.3.3 Evolution Variables

As we have mentioned, the choice of evolution variable Q^2 is not unique. Early versions of Pythia, for example, utilized $Q^2 = |m^2|$. We notice however that because the integration measure contains a $dz\ dQ^2/Q^2$, any variable of the form $Q^2 = f(z)m^2$ [35] recovers the same measure $dz\ dm^2/m^2$. The difference appears in the way that the shower probes the possible phase space. The current version of Pythia utilizes a measure of the transverse momentum of a final state evolution, namely

$Q^2 = p_\perp^2 = z(1-z)m^2$, with variations for initial state evolution according to kinematics which we will not discuss here. Many examples of evolution variables can be found in Refs. [5, 14, 32, 33, 35] but here we will discuss one important consequence of the choice.
While the parton shower algorithms implement the DGLAP splitting kernels which are only accurate in the collinear regime, it is very well known [21, 37], that when one analyzes the radiative corrections in a coherent manner; including interference effects due to soft emissions; the subsequent radiation patterns are, in a statistically averaged sense, non-zero only if the $(n+1)^{th}$ emitted parton is more collinear to its parent than the n^{th} parton is. This is an artefact of destructive interference and is recovered through the use of a clever evolution variable. The Herwig generator, for example, uses $Q^2 = m^2/(2z(1-z))$, which is related to the angle of emission [14] and therefore orderings in this variable approximately reproduce coherence effects. Pythia6 evolution is ordered in virtuality, which does not correspond to angle, however coherence effects are reproduced by implementing a veto on emissions violating angular ordering. Conversely, Pythia8 implements a measure of the transverse momentum of the branching, which is related to the angle of emission but also has advantages in describing hadron collisions [35]. Shown in Figure 2.5 are comparisons between Pythia6 and experimental data from the Collider Detector at Fermilab (CDF), with and without the angular ordering veto. It is clear that while agreement is not always obtained, the general trend is toward improvement, when a veto is included.

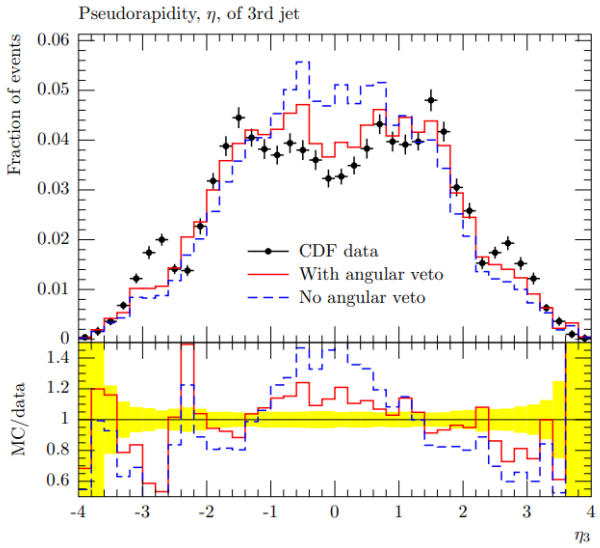

Figure 2.5: Pythia6 predictions of pseudorapidity, $\eta = -\ln(\tan\theta/2)$ where θ is the angle of the chosen particle from the beam axis, of a jet compared to CDF data from a pp collision at 1.8 TeV. Reproduced from [14] (Figure 4). CDF data from the Tevatron [36].

As a final note, in traditional parton showers the phase space measure $\mathrm{d}\Phi \sim \mathrm{d}t\ \mathrm{d}z$ of (2.3.5) is, just like the splitting kernels themselves, derived [21][7] under a small angle approximation. The phase space measure is therefore approximate and as a consequence, the implementation of evolution through phase space has unpopulated dead-zones, whereas the antenna formalism we are about to introduce implements an exact factorization of the phase space [16, 38] which mitigates this flaw.

[7] pp. 158-164

2.4 Antenna Showers

The antenna shower is based on $2 \to 3$ kinematics as opposed to the $1 \to 2$ of the parton shower. The algorithm is essentially the same except that the splitting kernel captures both the leading collinear and soft singularities, namely that the function f in Eq. (2.3.3) is denoted a for antenna function and is evaluated exactly as the ratio of the Born+1 amplitude squared to the Born level amplitude squared

$$a = \frac{|\mathcal{M}_{n+1}|^2}{|\mathcal{M}_n|^2} \tag{2.4.1}$$

For concreteness, the helicity averaged emission of gluons from a quark-antiquark pair in an 'Initial-Final' configuration (Fig. 2.7), so that $AK \to ajk$ for j a gluon, has an antenna function of the form [16][8]

$$a \sim \frac{1}{s_{AK}} \left(\underbrace{\frac{2s_{ak}s_{AK}}{s_{aj}s_{ak}}}_{\text{eikonal}} + \underbrace{\frac{s_{aj}}{s_{ak}} + \frac{s_{ak}}{s_{aj}}}_{\text{collinear}} \right) \tag{2.4.2}$$

where we have expressed it in the invariants often used in the literature, defined as $s_{\alpha\beta} = 2p_\alpha.p_\beta$. We have described what the antenna shower captures that the parton shower does not, so before continuing we will note some of the effects that the antenna formalism explicitly does *not* capture. The first term in Eq. (2.4.2) is the universal (massless) eikonal factor appearing in all antennae, and the others are collinear terms which depend on the spins of the particles involved and, as we will see, need not all appear. As we have mentioned, there may in addition be a finite process-dependent term such as a +1 or +2, which is omitted here.

An enlightening discussion on the general forms may be found in Ref. [33], but since the nonsingular terms are not universal, the working form of the antenna function for a given branching process is generally taken with whatever nonsingular addition is necessary to ensure positive definiteness. Therefore, as one generates a variety of different processes in the evolution of a shower, each branching will carry the leading antenna singularities, but there will be some amount of uncertainty in the final state associated with the differing nonsingular terms. Furthermore the antenna shower consists of coherent radiation from a dipole - what is not captured, however, is the coherent radiation from quadrupoles and other higher multipoles. This is due to the leading colour limit implemented in Vincia's shower algorithm, where the number of colours is taken infinite, and

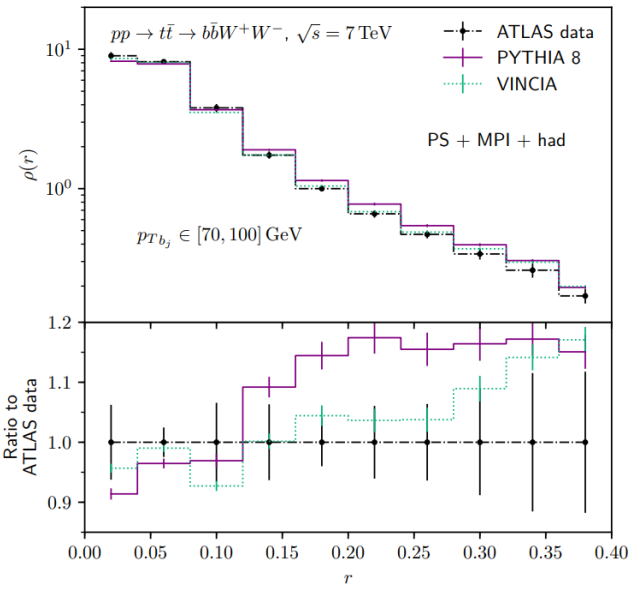

Figure 2.6: A plot of the b-jet distribution in a top decay event from ATLAS, with the ratio to ATLAS data in the lower subfigure. Reproduced from [38], Figure 11.

[8] Eq. 33

interference effects between dipoles become vanishingly small. This approximation is accurate to at least $1/N_C^2 \sim 10\%$ [15]. Comparisons of the Vincia shower to ATLAS data and the parton shower of Pythia 8 can be seen in Figure 2.6 and in most regions it appears that Vincia does perform slightly better. One single plot of course, is hardly enough to conclude superiority but nonetheless from an analytical point of view, the antenna shower does capture more information in the evolution than the parton shower.

Returning now to the details of the antenna shower, the Sudakov factor is of the general form

$$\Delta(Q_1^2, Q_2^2) = \exp\left(-\int_{Q_1^2}^{Q_2^2} \mathrm{d}\Phi_{\mathrm{ant}} 4\pi\alpha_s \mathcal{C}\bar{a}\right) \tag{2.4.3}$$

where $\mathcal{C}$ is a colour factor for the process in question, and $\bar{a}$ is a stripped antenna function, containing no coupling factor or colour factors. There is an implicit sum over all possible processes that can occur, and we are omitting factors due to parton distribution functions which are included in [16]. The phase space $\mathrm{d}\Phi_{\mathrm{ant}}$ is the phase space allowed to the $2 \to 3$ branching, the derivation of which we outline in Chapter 3.1.

We have not made any mention however, of the different types of $2 \to 3$ branching processes. Shown in Figure 2.7 are the final-final (FF) antenna, initial-final (IF) antenna, and initial-initial (II) antenna. Each has its own choice of conventions and evolution variable which vary slightly. However the FF, IF and II antennae are implemented to describe radiation following hard processes. We are interested in a special case of the IF antenna, namely the resonance-final (RF) antenna, wherein the 'initial' state is a resonance state like the top quark.

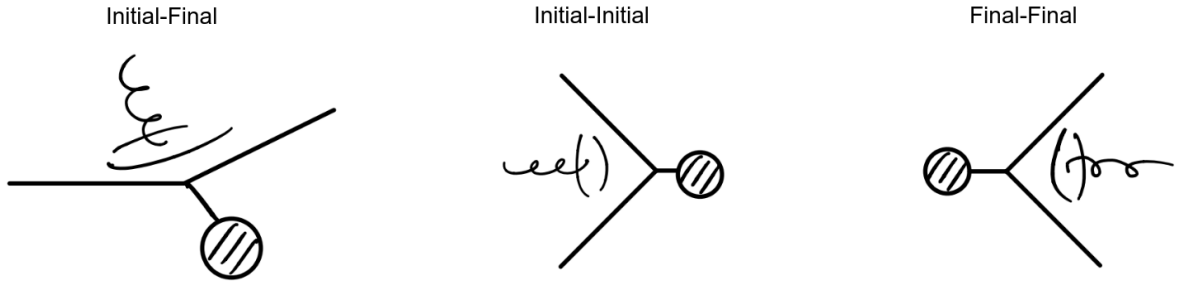

Figure 2.7: The three types of antenna functions. The lined circle represents an arbitrary process which we are not interested in.

Now, if we understand that the branching phase space is three dimensional (we will prove this shortly), it is instructive to consider these as the three degrees of freedom (DOF) of the emitted gluon. One useful decomposition of these DOF is into some angle ϕ around the axis of the original emitter, and some momentum components transverse and longitudinal with respect to the emitter. The transverse momentum is related to the resolution scale Q^2, for instance a gluon emitted with very small transverse momentum $p_\perp$ is harder to resolve from the parent than one with a high $p_\perp$. The longitudinal momentum is related to the z variable of the shower, and as we have discussed in Chapter 2.3.3, a given algorithm may implement a different specific choice for Q^2, z and ϕ.
Specifically, in the RF antenna implemented recently into Vincia [38], which we will study extensively later, the evolution variable is a transverse momentum. The physical interpretation is not particularly obvious from the form of the expression, however we include an example here for

completeness. Namely, for the emission of a gluon from a quark and the splitting of a gluon into quarks of m_q the evolution variables are respectively

$$Q^2_{\text{emit}} = \frac{s_{aj}s_{jk}}{s_{AK}+s_{jk}} \tag{2.4.4}$$

$$Q^2_{\text{split}} = \frac{(s_{aj}-m_q^2)(s_{jk}+2m_q^2)}{s_{AK}+s_{jk}+2m_q^2} \tag{2.4.5}$$

This shower also requires a splitting variable, similar to z in the parton shower which we will call ζ. Now, unlike the parton shower, the phase space measure of the antenna shower is exact and therefore one is free to choose some convenient functional form for ζ (i.e. that integrates faster), given that the appropriate Jacobian factor for the coordinate transformation is included. The specific choices, in this case, are

$$\zeta_{\text{emit}} = \frac{s_{jk}+s_{AK}}{s_{AK}} \tag{2.4.6}$$

$$\zeta_{\text{split}} = \frac{s_{ak}}{s_{AK}} \tag{2.4.7}$$

Let us now turn our discussion to the specific antenna function that we will study.

2.5 Scalar Quark Decay

The theory of Supersymmetry (SUSY), which we will not discuss in more depth than is presented here, is a well known and well studied extention of the Standard Model (SM). Motivated by its principal hypothesis, that for each fundamental fermion or boson in the SM there exists a corresponding ('superpartner') boson or fermion respectively, we will extend the treatment of coherent QCD radiation in the antenna formalism to the case of spin-0, or scalar, quarks. In the context of SUSY these are known as 'squarks' and we will often refer to them as such, however we emphasize that our treatment of them is independent of the specific paradigm for new physics in which they originate. We will formulate our results on the basis of spin structure alone, so that our findings will hold for any BSM model featuring spin-0 colour-triplet particles.

Nonetheless, for definiteness and to derive the antenna functions for scalar quarks within a well-defined QFT framework, we do take a supersymmetric extension of the SM as our reference case. For illustrative purposes we shall compare the radiation pattern emitted in the SM process $t \to bW$ to its would-be supersymmetric analogue of $\tilde{t} \to b\tilde{\chi}^+$. The $\tilde{t}$ is called a stop quark and the $\tilde{\chi}^+$, a chargino (having an antiparticle $\tilde{\chi}^-$), which we take to be a pure partner of the W boson. In our study we will keep all SUSY masses, couplings, and widths the same as their SM counterparts, i.e. $m_{\tilde{t}} = m_t$, $m_{\tilde{\chi}} = m_W$. Since a stop quark has never been observed it follows that it must have a much larger production threshold, i.e. a larger mass, so while our assumption is not phenomenologically viable, it is a useful construction that simplifies the derivation of the antenna function, as well as our study of how the spin structure of an event inflences its radiation pattern. We stress again that our formalism is universal, and hence our results are independent of the particular SUSY model that is being used.

Chapter 3

Deriving the Antenna Function

The decay of the stop quark is shown in Figure 3.1. On the left of the Figure, we have the Born level decay, where a stop decays into a bottom and a chargino. An important detail here is that while the stop and the bottom are coloured particles, the chargino is not.

We then consider the Born+1 process, wherein a gluon is emitted from the colour dipole between the stop and the bottom quark. We will write this $\tilde{t} \to b + \tilde{\chi} + g$ and the two possibilities are shown in the right hand side of Figure 3.1. Note that unless there is an explicit need for it, we will often suppress the $^+$ superscript on the $\tilde{\chi}$ for economy. With these we construct the antenna function according to Equation 2.4.1.

Now, each external line in these diagrams carries some helicity, or in the case of the gluons, a polarization. Likewise, each line carries some colour. Since we cannot observe a particular colour state, and we are not interested at this stage at the probability amplitude of a specific helicity configuration, we will compute the colour and helicity averaged amplitude by summing over the colours and helicities of the outgoing particles and averaging over the colours and helicities of the incoming particles. We will make explicit mention of this in the derivation that follows.

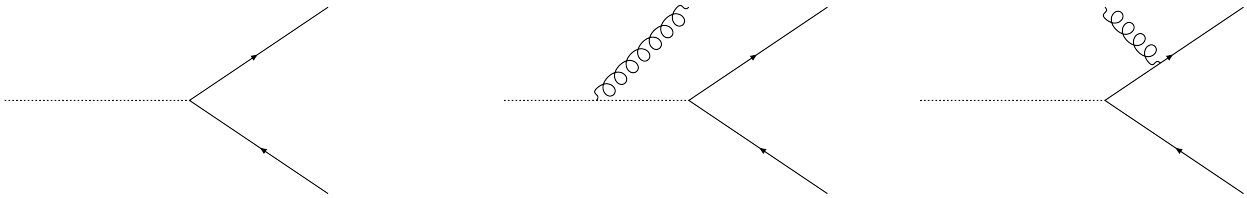

Figure 3.1: The stop decay process, with the Born level on the left and with the two possible radiative corrections on the right. The dashed line is the stop quark, the solid upper line is the bottom quark, and the lower solid line is the chargino.

3.1 Conventions, Kinematics, and Phase Space

To define the branching we require a 'kinematics map' relating the post-branch system to the pre-branch system. We will impose, as in [16, 38] that momentum is conserved locally within each branching. Since we are considering an 'initial-final' type antenna, we match the conventions of [16, 32]: in Figure 3.2 we have let the particles of the initial state have momenta p_A, p_K, p_X,

and those of the final state have momenta p_a, p_j, p_k and p'_X. The X can stand for any system of recoilers but in our derivation we will take this to be simply a spin-1/2 fermion of mass m_X.
The kinematics map relating the pre-branching to the post-branch system is illustrated in Figure 3.2, and can be understood in the following way: initially we make a $2 \to 3$ map to split the AK partons into ajk, such that p_X is unchanged. Following this, we boost back into the center of mass frame of a so that effectively, the X particle picks up some recoil $p'_X - p_X$ to become p'_X. Likewise, the k parton is re-oriented following the boost so that in the final state, the transverse momentum is shared between the two ends of the original dipole. Conversely, recoil strategies in parton showers impart a recoil to only one parent, and therefore this kinematics map is unique to our formalism.

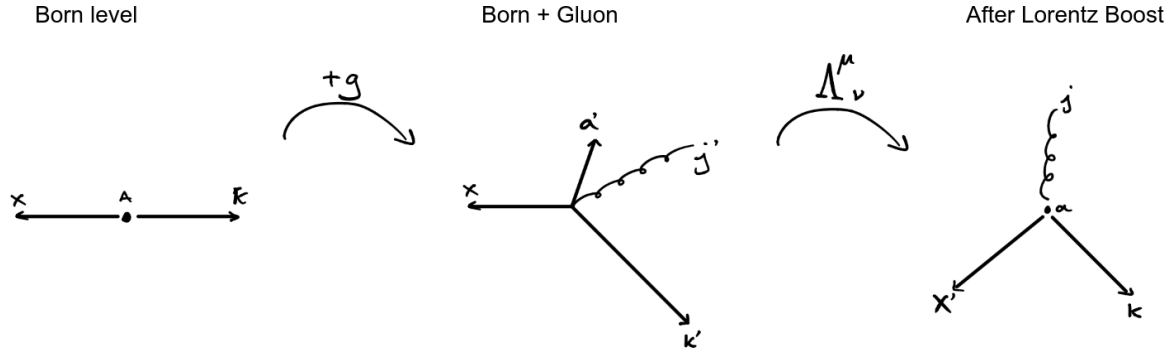

Figure 3.2: In the Born level process the decay products move anticollinearly. Following gluon emission the A and K parton transform into a, j, and k. Applying an appropriate Lorentz boost Λ, we map back into the rest frame of a to provide X and K with an effective trasnverse recoil.

Consider now the phase space of the process. The well known expression for the Lorentz invariant phase space for a particle a of mass M to decay into two particles $a \to bc$ [20, 39]:

$$\mathrm{d}\Phi_2\left(p_a; p_b, p_c\right) = \delta^{(4)}\left(p_a - p_b + p_c\right) \frac{\mathrm{d}^3 p_b}{(2\pi)^3 2E_b} \frac{\mathrm{d}^3 p_c}{(2\pi)^3 2E_c} \tag{3.1.1}$$

This is easily extended to an n-body decay:

$$\mathrm{d}\Phi_n\left(p_a; p_1, ..., p_n\right) = \delta^{(4)}\left(p_a - \sum_{i=1}^{n} p_n\right) \prod_{i=1}^{n} \frac{\mathrm{d}^3 p_i}{(2\pi)^3 2E_i} \tag{3.1.2}$$

and can be expressed in a particularly useful way, namely through a recursive relation. For further details we refer the reader to [40].[1] Suppose we have a j-body decay, where one of the daughters then undergoes a k-body decay so that the final state has n bodies. We must have that $(j-1)+k = n$, and the net phase space is written in factorized form:

$$\mathrm{d}\Phi_n\left(p_a; p_1, ..., p_n\right) = \mathrm{d}\phi_j(q; p_1, ..., p_j) \;\times\; \mathrm{d}\phi_{n-j+1}\left(p_a; q, p_{j+1}, ..., p_n\right) (2\pi)^3 \, dq^2 \tag{3.1.3}$$

with $q^2 = (\sum_{i=1}^{j} E_i)^2 - |\sum_{i=1}^{j} \vec{p}_i|^2$. Using this one may construct the phase space of the branching in terms of the phase spaces of the 'before' and 'after' processes, which is precisely what we have described in the Introduction. We will briefly demonstrate how this is done, however formal treatments can be found in [41, 42].

[1] Chapter 47

We may write the 2-body phase space in the rest frame of the parent as

$$\mathrm{d}\Phi_2 = \frac{1}{4(2\pi)^6}\frac{|\vec{p}_1|}{M}\ \mathrm{d}\alpha\ \mathrm{d}\cos\beta \tag{3.1.4}$$

where the angular measures correspond to the global orientation of the dipole axis, M is the mass of the original decayer, and $\vec{p}_1$ is the momentum of either of the daughters. The equivalent 3-body phase space, after averaging over helicities is

$$\mathrm{d}\Phi_3 = \frac{1}{4(2\pi)^7}\mathrm{d}E_1\mathrm{d}E_2\frac{\mathrm{d}\phi}{2\pi}\mathrm{d}\alpha'\ \mathrm{d}\cos\beta' \tag{3.1.5}$$

where E_1 and E_2 are the energies of two of the daughters in the rest frame of the decayer, and α', β', ϕ are the three Euler angles of the rigid body. We are free to set the 2-body system to lie on the same plane as the 3-body system, which effectively allows us to eliminate the dependence of the branching phase space on α and α'. Remaining in the 3-body system are the angles ϕ and β'. The ϕ angle defines the global orientation of the branching plane, which we keep. The relation between β and β' must then be understood. In the context of the branching phase space, these simply correspond to the recoil angles aquired by the post-decay partons relative to the pre-decay partons. Therefore in the antenna phase space this reduces to some angular separation Ψ_{Kk} between the pre-branch parton K and the post branch one k, which in general is not unique. That is, our branching phase space is actually a one-parameter family of possible phase spaces, $[\mathrm{d}\Phi_3/\mathrm{d}\Phi_2](r)$, for some real number r.
In the context of a shower algorithm, however, a unique recoil angle is constrained by the kinematics map applied. Therefore we have for some r_0,

$$\mathrm{d}\Phi_{\mathrm{ant}} = \int [\frac{\mathrm{d}\Phi_3}{\mathrm{d}\Phi_2}](r)\ \delta(r - r_0)\ \mathrm{d}r \tag{3.1.6}$$

Following this through one can compute the antenna phase space as

$$\mathrm{d}\Phi_{\mathrm{ant}} = \frac{1}{8\pi^2}\frac{M}{|\vec{p}_1|}\ \mathrm{d}E_1\mathrm{d}E_2\frac{\mathrm{d}\phi}{2\pi} \tag{3.1.7}$$

It is then a matter of tedious Jacobians to transform from this form into

$$\mathrm{d}\Phi_{\mathrm{ant}} = \frac{1}{16\pi^2 s}\mathrm{d}s_{aj}\mathrm{d}s_{jk}\frac{\mathrm{d}\phi}{2\pi} \tag{3.1.8}$$

where $s_{ab} := 2p_a.p_b$ and, in this context, we will use $s = s_{jk} + s_{AK}$.

3.2 SUSY Model Independence

To compute the antenna function we will not require a full supersymmetric model. In any process, the vertices of the Feynman diagrams each carry a factor of the field-couplings. Where the gluon connects to either the stop or the bottom, we will have a factor of the strong coupling, g_s. Where the stop splits into the bottom and the chargino however depends on the supersymmetric coupling $g_{\tilde{t}b\tilde{\chi}}$. However, the definition of the antenna function allows us to bypass the need to know such a coupling, and indeed to bypass a full supersymmetric treatment altogether. The two diagrams in the numerator each contain a factor of g_s and a factor of $g_{\tilde{t}b\tilde{\chi}}$, and the diagram in the denominator

contains only a factor of $g_{\tilde{t}b\tilde{\chi}}$. When these diagrams are added up and the squares taken, the overall factors of $g^2_{\tilde{t}b\tilde{\chi}}$ will cancel between the numerator and the denominator, which will leave an overall factor of g_s^2 for the antenna function. The consequence of this is that we need only consider the spin structure of such an amplitude, and disregard the other properties of the particles themselves. That is to say, we may calculate the antenna function by considering the decay of an an arbitrary coloured spin-0 particle into an arbitrary pair of spin-1/2 particles, one coloured and one colourless.

3.3 Feynman Rules

We will implement an extension of a theory known as scalar quantum chromodynamics (sQCD), where an example in 2 dimensions may be found in Ref [43]. In sQCD we have quarks coupling to gluons, except that the quarks are treated as having spin-0, not 1/2. In our toy theory, we will combine the sQCD picture with the QCD one, so that we have both fermionic and scalar quarks. To reproduce the $\tilde{t}b\tilde{\chi}$ vertex, we require in addition a colourless fermion to model the $\tilde{\chi}$. We will let ϕ_i be the field of the stop quark with colour i. Using ψ for the fermions we let ψ_i be the field of a bottom quark with colour i, and ψ the chargino. To construct the coupling, we see that it can take no other form than $\phi_i\bar{\psi}\psi_i$: this is the only Lorentz invariant and colour-conserving vertex we can construct out of the three fields.
We couple the scalar particle to the gluon field in a gauge invariant manner by virtue of a covariant derivative $(D_\mu\phi_i)(D^\mu\phi_i^*)$, the fermion ψ_i is just a quark so couples in the same way as the original QCD Lagrangian (2.1.4), and the fermion ψ is an arbitrary fermion with a Dirac Lagrangian $\bar{\psi}(i\partial\!\!\!/ - m)\psi$. We note also the existence of the scalar antiparticle ϕ_i^* so that our Lagrangian is

$$\mathcal{L} = \mathcal{L}_\psi + \mathcal{L}_{\text{QCD}} + \mathcal{L}_{\text{sQCD}} + g(\phi_i\bar{\psi}\psi_i + \phi_i^*\bar{\psi}_i\psi) \tag{3.3.1}$$

As noted above, the amplitude will be independent of the actual value of this coupling. So, while strictly incorrect - we will use $g = g_s$ to avoid cluttering up intermediate results, particularly in the calculations with factors like $g^2g_s^2$.

In identifying the appropriate Feynman rules, we refer to the appendices of Peskin & Schroeder [39] or Griffiths [23] which detail all the rules pertinent to our Lagrangian, except for the vertices $\phi_i \to \bar{\psi}_i\psi$ and $\phi_i \to g + \phi_j$ where g is a gluon. In Appendix C we derive these vertex factors and state all the Feynman rules which we utilize in the following section.

3.4 Born Level

We will first calculate the Born level squared amplitude, as displayed in Figure 3.3. We will let the incoming scalar particle have colour i and let the outgoing quark have colour j. Let the quark have spin r and let the colourless fermion have spin s. Using the Feynman rules listed in Appendix C we construct the amplitude, where again we stress that, while strictly incorrect, we have set the SUSY coupling $g_{\tilde{t}b\tilde{\chi}} = g_s$ since our final result is independent of $g_{\tilde{t}b\tilde{\chi}}$.[2] In our case we will take the mass of the b quark, $m_K = 0$ for simplicity. When we finally obtain the antenna function we can exploit universality to insert the appropriate mass-correction term.
We will here drop the momentum labels for clarity and in the end make the appropriate substitu-

[2] Arguably $g_{\tilde{t}b\tilde{\chi}} = 1$ is an even cleaner choice, however we have opted for g_s instead, so that the order of perturbation theory is still indicated in the amplitudes themselves.

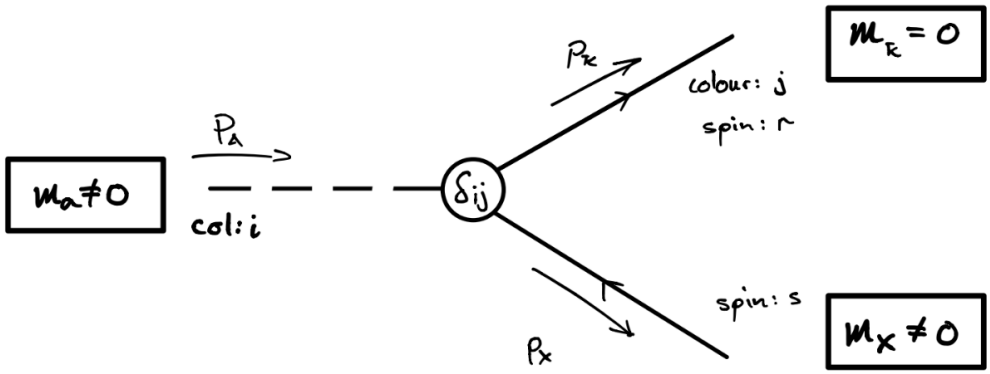

Figure 3.3: $i\mathcal{A} = \bar{u}_j^r(p_K)\ ig_s\delta_{ij}\ v^s(p_X)$

tions. We have the squared probability amplitude as

$$|\mathcal{M}|^2 = \left(\bar{u}_j^r\ ig_s\delta_{ij}\ v^s\right)^* \left(\bar{u}_j^r\ ig_s\delta_{ij}\ v^s\right) \tag{3.4.1}$$

$$= g_s^2\delta_{ij}\delta_{ij}\left(\bar{u}_j^r v^s\right)^* \left(\bar{u}_j^r v^s\right) \tag{3.4.2}$$

where our amplitude at this stage carries an implicit colour index j. Now, since $\bar{u}v$ is an inner product, we have $(\bar{u}v)^* = (\bar{u}v)^\dagger = v^\dagger(u^\dagger\gamma^0)^\dagger = v^\dagger(\gamma^0)^\dagger u = v^\dagger\gamma^0 u = \bar{v}u$. Therefore Eq. (3.4.2) becomes

$$|\mathcal{M}|^2 = g_s^2\delta_{ij}\delta_{ij}(\bar{v}^s u_j^r \bar{u}_j^r v^s) \tag{3.4.3}$$

We now wish to sum over outgoing colours and average over incoming colours. The sum over outgoing colours is a straightforward $\sum_{j=1}^3$, while averaging over the incoming colours amounts to a $\frac{1}{3}\sum_{i=1}^3$. We therefore have

$$|\mathcal{M}|^2 = \frac{1}{3}\sum_{i=1}^3\sum_{j=1}^3 g_s^2\delta_{ij}\delta_{ij}(\bar{v}^s u_j^r \bar{u}_j^r v^s) \tag{3.4.4}$$

$$= \frac{1}{3}\sum_{i=1}^3 g_s^2\delta_{ii}(\bar{v}^s u_i^r \bar{u}_i^r v^s) \tag{3.4.5}$$

$$= g_s^2(\bar{v}^s u^r \bar{u}^r v^s) \tag{3.4.6}$$

Where the coloured spinors u_i have been absorbed into a colourless spinor u with an overall factor 3 cancelling the $1/3$.[3]

Let us now sum over the helicities of the outgoing fermions, r. We use the spinor outer product identities for fermions of mass m and momentum p [20]:

$$\sum u^s(p)\bar{u}^s(p) = (\not{p} + m) \tag{3.4.7}$$

$$\sum v^s(p)\bar{v}^s(p) = (\not{p} - m) \tag{3.4.8}$$

Summing over the helicities of the massless u spinor then,

$$\sum_{r=-1,1} |\mathcal{M}|^2 = g_s^2\left(\bar{v}^s \not{p}_K v^s\right) \tag{3.4.9}$$

[3]Note that the definition of the coloured spinor is $u_i = uc_i$ where c_i is a triplet in colour space, so that summing over colours gives a multiplicative factor of 3.

To simplify this, we note a general identity which will be of use in calculating the Born+1 squared matrix elements as well. Consider an arbitrary inner product of the form as in Eq. (3.4.9), for an arbitrary spinor v and an arbitrary matrix Q. Rewriting this with explicit componentwise summation,

$$\bar{v}Qv = \sum_{i,j} \bar{v}_i Q_{ij} v_j = \sum_{i,j} v_j \bar{v}_i Q_{ij} = \mathrm{Tr}(v\bar{v}Q) \tag{3.4.10}$$

We thus rewrite (3.4.9) as

$$|\mathcal{M}|^2 = g_s^2 \,\mathrm{Tr}\left(v^s \bar{v}^s \not{p}_K\right) \tag{3.4.11}$$

Now we may utilize outer product identities. The v spinor is a final-state particle so we sum over the helicities to obtain the helicity averaged matrix element squared. Unlike the u spinor, this is not massless. We therefore have

$$\overline{|\mathcal{M}|}^2 = g_s^2 \,\mathrm{Tr}\left(\left(\not{p}_X - m_X\right)\not{p}_K\right) \tag{3.4.12}$$

$$= g_s^2 \,\mathrm{Tr}\left(\not{p}_X \not{p}_K - m_X \not{p}_K\right) \tag{3.4.13}$$

We know [39] that a trace of any odd number of slashed matrices is zero, and that $\mathrm{Tr}\,(\not{a}\not{b}) = 4a.b$, so

$$\overline{|\mathcal{M}|}^2 = g_s^2 \,\mathrm{Tr}\left(\not{p}_X \not{p}_K\right) \tag{3.4.14}$$

$$= 4g_s^2 p_X.p_K \tag{3.4.15}$$

From momentum conservation,

$$\overline{|\mathcal{M}|}^2 = 4g_s^2 (p_A - p_K).p_K \tag{3.4.16}$$

$$= 4g_s^2 p_A.p_K \tag{3.4.17}$$

where we have used the on shell condition of the massless outgoing quark $p_K^2 = 0$. We finally obtain the squared Born level matrix element squared

$$|\mathcal{M}|^2 = 4g_s^2 \; p_A.p_K \tag{3.4.18}$$

3.5 Radiative Corrections

We consider now the radiative correction to the Born process whereby a gluon is emitted off one of the coloured particles. We have the following two processes with amplitudes as given in Figures 3.4 and 3.5.

We therefore have to calculate

$$\left| \quad + \quad \right|^2 = \left| \quad \right|^2 + 2\,\mathrm{Re}\left[\left(\quad \right)^* \left(\quad \right)\right] + \left| \quad \right|^2 \tag{3.5.5}$$

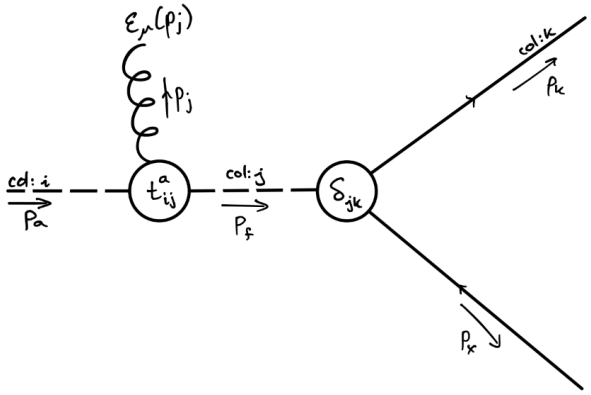

Figure 3.4: Born+1 with scalar radiation

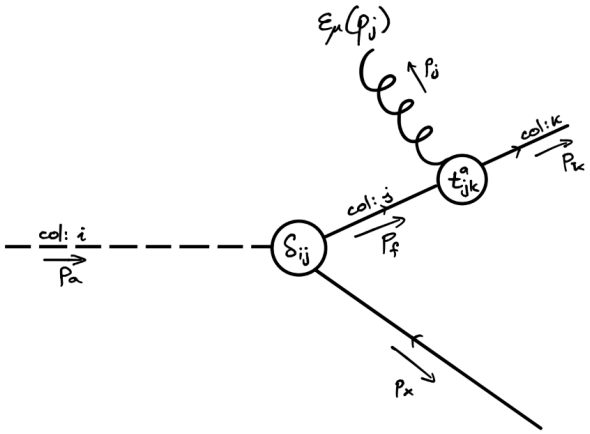

Figure 3.5: Born+1 with fermion radiation

$$i\mathcal{A} = \bar{u_k}\ ig_s\delta_{jk}\frac{i}{p_s^2 - m_a^2}\ v\ ig_s t^a_{ij}(p_a + p_s)^\mu \varepsilon^*_\mu \tag{3.5.1}$$

$$= -i\ \frac{g_s^2}{p_s^2 - m_a^2}\left[\bar{u}_k v\right](p_a + p_s)^\mu \varepsilon^*_\mu \delta_{jk} t^a_{ij} \tag{3.5.2}$$

$$i\mathcal{A} = \bar{u}_k\ ig_s t^a_{jk}\ \gamma^\mu \varepsilon^*_\mu \frac{i\left(\not{p}_f + m_j\right)}{p_f^2 - m_j^2}\ ig_s\delta_{ij} v \tag{3.5.3}$$

$$= -i\ \frac{g_s^2}{p_f^2}\left[\bar{u}_k \gamma^\mu \varepsilon^*_\mu \not{p}_f v\right]\delta_{ij} t^a_{jk} \tag{3.5.4}$$

We will make use the following notation to denote squared amplitudes:

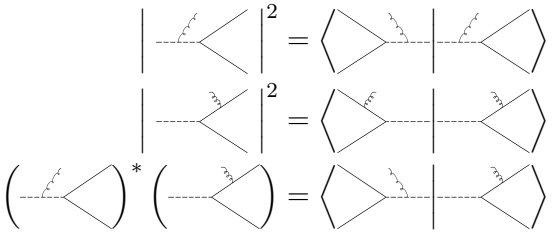

(3.5.6)

(3.5.7)

(3.5.8)

We will at times refer to the complex conjugated term, i.e. the 'bra' in Equations (3.5.6)-(3.5.8) as the 'bra-diagram' and the non-conjugated term, i.e. the 'ket' as the 'ket-diagram.'
As a disclaimer, we have continued as per convention to use i, j, k for the colour indices, however with a slight abuse in notation, we also label the momenta with subscripts p_j and p_k. However since we suppress the p_j and p_k within the spinors until after summing over colours, there is no risk of confusion here.

3.5.1 Radiation from the Scalar

From Figure 3.4 we have

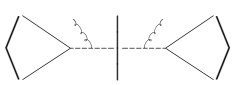

$$= \left(-i\ \frac{g_s^2}{p_s^2 - m_a^2}\left[\bar{u}_k v\right](p_a + p_s)^\nu \varepsilon^*_\nu \delta_{lk} t^a_{il}\right)^* \left(-i\ \frac{g_s^2}{p_s^2 - m_a^2}\left[\bar{u}_k v\right](p_a + p_s)^\mu \varepsilon^*_\mu \delta_{jk} t^a_{ij}\right) \tag{3.5.9}$$

where we have a different colour index for the off-shell propagator particle in the bra-diagram as to the ket-diagram, but the in and outgoing particles have the same colours. Collecting terms and

using the Hermiticity of the t Matrices to write $(t^a_{ij})^* = (t^a_{ij})^T$, we have

$$= \frac{g_s^4}{(p_s^2 - m_a^2)^2} \left[\bar{v} u_k \bar{u}_k v\right] (p_a + p_s)^\mu (p_a + p_s)^\nu \varepsilon_\mu \varepsilon^*_\nu \left(\delta_{jk} t^a_{ji} t^a_{il} \delta_{lk}\right) \tag{3.5.10}$$

To sum and average over colours we divide by 3 for the i index, and sum over the j, k, l, a indices.

$\therefore$ $\frac{1}{3} \sum_{a,i,j,k,l=1}^{3}$ 

$$= \frac{g_s^4}{3(p_s^2 - m_a^2)^2} \sum_{a,i,j,k,l=1}^{3} \left[\bar{v} u_k \bar{u}_k v\right] (p_a + p_s)^\mu (p_a + p_s)^\nu \varepsilon_\mu \varepsilon^*_\nu \left(\delta_{jk} t^a_{ji} t^a_{il} \delta_{lk}\right) \tag{3.5.11}$$

The sum over j fixes $j = k$, while the sum over l fixes $l = k$, leaving

$\frac{1}{3} \sum_{a,i,j,k,l=1}^{3}$ 

$$= \frac{g_s^4}{3(p_s^2 - m_a^2)^2} \sum_{a,i,k=1}^{3} \left[\bar{v} u_k \bar{u}_k v\right] (p_a + p_s)^\mu (p_a + p_s)^\nu \varepsilon_\mu \varepsilon^*_\nu \left(t^a_{ki} t^a_{ik}\right) \tag{3.5.12}$$

And summing over u_k introduces an overall factor of 3 to cancel that in the denominator and leaves a spinor outer product. Finally summing over a and i we have

$$\sum_{a,i,k} t^a_{ki} t^a_{ik} = \mathrm{Tr}\left\{\sum_a t_a t_a\right\} = 4 \tag{3.5.13}$$

Where the value of 4 is a consequence of our choice of convention for the t matrices and is consistent with our Feynman rules. We will drop the summation signs on the left hand side and continue to write[4]

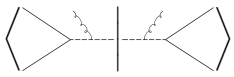

$$= \frac{4g_s^4}{(p_s^2 - m_a^2)^2} \left[\bar{v}(\not{p}_k) v\right] (p_a + p_s)^\mu (p_a + p_s)^\nu \varepsilon_\mu \varepsilon^*_\nu \tag{3.5.14}$$

Let us now sum over the helicities of the v spinors. As shown earlier, this generates a trace over the spinors to give

$$= \frac{4g_s^4}{(p_s^2 - m_a^2)^2} \mathrm{Tr}\left[\left(\not{p}_X - m_X\right) \not{p}_k\right] (p_a + p_s)^\mu (p_a + p_s)^\nu \varepsilon_\mu \varepsilon^*_\nu \tag{3.5.15}$$

$$= \frac{4g_s^4}{(p_s^2 - m_a^2)^2} 4 p_X . p_k \, (p_a + p_s)^\mu (p_a + p_s)^\nu \varepsilon_\mu \varepsilon^*_\nu \tag{3.5.16}$$

We are now interested in summing over the polarizations of the outgoing gluon. We will use the Ward identity which, strictly speaking is not an identity but a replacement rule, whereby summing over polarization vectors amounts to identification

$$\sum_\varepsilon \varepsilon_\mu \varepsilon^*_\nu \to -g_{\mu\nu} \tag{3.5.17}$$

Before summing over the polarizations of the outgoing spins, we will point out a naïve use of the identity. Recall the consequence of the Lorenz gauge, namely $\varepsilon_\mu(p) p^\mu = 0$. In the product of

[4]Note that in what follows we will frequently absorb our sums over colours and polarizations into the overall symbol for the amplitude without comment.

momenta in the amplitude we have $p_a + p_s$. Now, $p_s = p_a - p_j$ is the momentum of the off-shell scalar, which substitutes to give

$$p_a + p_s = 2p_a - p_j \tag{3.5.18}$$

Therefore, we have

$$(p_a + p_s).\varepsilon(p_j) = (2p_a - p_j).\varepsilon(p_j) = 2p_a.\varepsilon(p_j) \tag{3.5.19}$$

So that the amplitude following summation becomes

$$\sum_{\varepsilon} \left\langle \quad \right| \quad \left. \right\rangle = \frac{4g_s^4}{(p_s^2 - m_a^2)^2}\ 4p_X.p_k\ \ (2p_a)^\mu\,(2p_a)^\nu \sum_{\varepsilon} \varepsilon_\mu(p_j)\varepsilon^*_\nu(p_j) \tag{3.5.20}$$

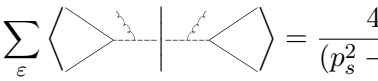

Summing over amplitudes therefore gives a factor of $-4p_a^2 = -4m_a^2$ by use of the Ward identity (3.5.17).

This, however, is an incorrect use of the identity. As stated, it is not an identity but a replacement rule that only holds after all the polarizations have been summed over. To use the Lorentz condition before this summation has been done amounts to losing information on the amplitude following the replacement. The correct use of the identity therefore requires us to first make the replacement. That is to say, we obtain

$$\begin{aligned}(2p_a - p_j)^\mu\,(2p_a - p_j)^\nu \varepsilon_\mu(p_j)\varepsilon^*_\nu(p_j) &\to -(2p_a - p_j).(2p_a - p_j) && (3.5.21)\\ &= -4p_a^2 + 4p_a.p_j - p_j^2 && (3.5.22)\\ &= -4(m_a^2 - p_a.p_j) && (3.5.23)\end{aligned}$$

We therefore see that we lose in the summation an additive $4p_a.p_j$ term. Understanding this, then, we have the helicity and colour averaged amplitude squared, which we will denote as

$$\overline{\quad \left\langle \quad \right| \quad \left. \right\rangle} = \frac{-4g_s^4}{(p_s^2 - m_a^2)^2}\ 4p_X.p_k\ 4(m_a^2 - p_a.p_j) \tag{3.5.24}$$

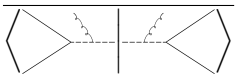

For p_X we have

$$\begin{aligned}p_X &= p_a - p_j - p_k && (3.5.25)\\ \implies p_X.p_k &= p_a.p_k - p_j.p_k - p_k^2 && (3.5.26)\\ &= p_a.p_k - p_j.p_k && (3.5.27)\end{aligned}$$

while for p_s we have

$$\begin{aligned}p_s &= p_a - p_j && (3.5.28)\\ \implies p_s^2 &= m_a^2 - 2p_a.p_j && (3.5.29)\end{aligned}$$

Making these substitutions gives

$$\begin{aligned}\overline{\quad \left\langle \quad \right| \quad \left. \right\rangle} &= \frac{-16g_s^4}{4(p_a.p_j)^2}\ 4(p_a.p_k - p_a.p_j)(m_a^2 - p_a.p_j) && (3.5.30)\\ &= -16g_s^4(m_a^2 - p_a.p_j)\left(\frac{p_j.p_k - p_a.p_k}{(p_a.p_j)^2}\right) && (3.5.31)\end{aligned}$$

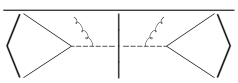

and we now have our first squared matrix element for the radiative correction.

3.5.2 Fermion radiated diagram squared

Now we turn our attention to the diagram in Eq. (3.5.7). From Figure 3.5 we have

$$= \left(-i\ \frac{g_s^2}{p_f^2}\left[\bar{u}\gamma^\mu\varepsilon_\mu^*\ \not{p}_f v\right]\delta_{il}t^a_{lk}\right)^* \left(-i\ \frac{g_s^2}{p_f^2}\left[\bar{u}\gamma^\mu\varepsilon_\mu^*\not{p}_f v\right]\delta_{ij}t^a_{jk}\right) \tag{3.5.32}$$

where we have dropped the colour indices on the u spinors, since we have seen above that they will be dropped at the stage of colour averaging. We simplify the conjugate similarly to the Born level diagram, with some extra complexity due to the gamma matrices within the inner product. Namely, for an arbitrary matrix Q, we have

$$(\bar{u}Qv)^* = (\bar{u}Qv)^\dagger = v^\dagger Q^\dagger (u^\dagger\gamma^0)^\dagger = v^\dagger\gamma^0\gamma^0 Q^\dagger\gamma^0 u = \bar{v}\gamma^0 Q\gamma^0 u \tag{3.5.33}$$

where we have made use of $\gamma^0\gamma^0 = 1$ and $(\gamma^0)^\dagger = \gamma^0$. Then, writing $\gamma^\mu\varepsilon_\mu^* = \not{\varepsilon}^*$, Eq. (3.5.32) becomes

$$= \frac{g_s^4}{p_f^4}\left[\bar{v}\gamma^0\left(\gamma^\mu\varepsilon_\mu^*\ \not{p}_f\right)^\dagger\gamma^0 u\right]\left[\bar{u}\not{\varepsilon}^*\not{p}_f v\right]\delta_{il}t^a_{kl}t^a_{jk}\delta_{ij} \tag{3.5.34}$$

The colour factor here is identical to that in Eq. (3.5.10), so that summation and averaging recovers the same prefactor, giving the colour averaged amplitude

$$= \frac{4g_s^4}{p_f^4}\left[\bar{v}\gamma^0\left(\gamma^\mu\varepsilon_\mu^*\ \not{p}_f\right)^\dagger\gamma^0 u\right]\left[\bar{u}\not{\varepsilon}^*\not{p}_f v\right] \tag{3.5.35}$$

$$= \frac{4g_s^4}{p_f^4}\left[\bar{v}\gamma^0\left(\left(\not{p}_f\right)^\dagger\varepsilon_\mu\left(\gamma^\mu\right)^\dagger\right)\gamma^0 u\right]\left[\bar{u}\not{\varepsilon}^*\not{p}_f v\right] \tag{3.5.36}$$

Since $\gamma_\mu^\dagger = \gamma^0\gamma_\mu\gamma^0$ it is easy to see that $\not{p}^\dagger = \gamma^0\not{p}\gamma^0$, giving

$$= \frac{4g_s^4}{p_f^4}\left[\bar{v}\gamma^0\left(\gamma^0\not{p}_f\gamma^0\varepsilon_\mu\gamma^0\gamma^\mu\gamma^0\right)\gamma^0 u\right]\left[\bar{u}\not{\varepsilon}^*\not{p}_f v\right] \tag{3.5.37}$$

$$= \frac{4g_s^4}{p_f^4}\left[\bar{v}\ \not{p}_f\not{\varepsilon}u\right]\left[\bar{u}\ \not{\varepsilon}^*\not{p}_f v\right] \tag{3.5.38}$$

Now isolate the polarization vectors so that we may apply the Ward identity

$$= \frac{4g_s^4}{p_f^4}\left[\bar{v}\ \not{p}_f\gamma^\mu\ u\bar{u}\ \gamma^\nu\not{p}_f v\right]\varepsilon_\nu^*\varepsilon_\mu \tag{3.5.39}$$

$$\implies \sum_\varepsilon$$

$$= -\frac{4g_s^4}{p_f^4}\left[\bar{v}\ \not{p}_f\gamma^\mu\ u\bar{u}\ \gamma_\mu\ \not{p}_f v\right] \tag{3.5.40}$$

Referring to the identity (3.4.10) derived for the Born amplitude, we rewrite this as

$$\sum_\varepsilon$$ 

$$= \frac{4g_s^4}{p_f^4}\,\mathrm{Tr}\left[v\bar{v}\ \not{p}_f\gamma^\mu\ u\bar{u}\ \gamma_\mu\ \not{p}_f\right] \tag{3.5.41}$$

We may finally sum over the helicities of u and v to write

$$= -\frac{4g_s^4}{p_f^4}\,\mathrm{Tr}\left[\left(\not{p}_X - m_X\right)\ \not{p}_f\gamma^\mu\ \left(\not{p}_k\right)\gamma_\mu\ \not{p}_f\right] \tag{3.5.42}$$

Using $\gamma^\mu \not{a} \gamma_\mu = -2\not{a}$, this reduces to

$$= \frac{8g_s^4}{p_f^4} \mathrm{Tr}\left[\left(\not{p}_X - m_X\right)\ \not{p}_f \not{p}_k \not{p}_f\right] \tag{3.5.43}$$

$$= \frac{8g_s^4}{p_f^4} \mathrm{Tr}\left[\not{p}_X \not{p}_f \not{p}_k \not{p}_f\right] \tag{3.5.44}$$

where in the last line, we have used that the trace of an odd number of gamma matrices is zero. Using $\mathrm{Tr}\left(\not{a}\not{b}\not{c}\not{d}\right) = 4\left(a.b\ c.d - a.c\ b.d + a.d\ b.c\right)$ we have

$$= \frac{32g_s^4}{p_f^4}\left(p_X.p_f\ p_k.p_f - p_X.p_k\ p_f^2 + p_X.p_f\ p_f.p_k\right) \tag{3.5.45}$$

Using conservation of momentum we have $p_X = p_a - p_j - p_k$, $p_f = p_j + p_k$ so

$$p_X.p_f = p_a.p_j + p_a.p_k - 2p_j.p_k \tag{3.5.46}$$

$$p_X.p_k = p_a.p_k - p_j.p_k \tag{3.5.47}$$

$$p_X.p_j = p_a.p_j - p_k.p_j \tag{3.5.48}$$

and

$$p_k.p_f = p_j.p_k \tag{3.5.49}$$

$$p_f.p_f = (p_f)^2 = 2p_j.p_k \tag{3.5.50}$$

$$\therefore\ (p_f)^4 = 4(p_j.p_k)^2 \tag{3.5.51}$$

This gives

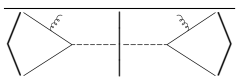

$$= \frac{32g_s^4}{4(p_j.p_k)^2}\left(2\left(p_a.p_j + p_a.p_k - 2p_j.p_k\right)p_j.p_k - 2\left(p_a.p_k - p_j.p_k\right)p_j.p_k\right) \tag{3.5.52}$$

$$= 16g_s^4\ \frac{p_a.p_j + p_a.p_k - 2p_j.p_k - p_a.p_k + p_j.p_k}{p_j.p_k} \tag{3.5.53}$$

Cleaning up, we have the helicity and colour averaged amplitude

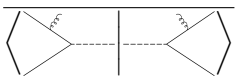

$$= 16g_s^4\ \frac{p_a.p_j - p_j.p_k}{p_j.p_k} \tag{3.5.54}$$

3.5.3 Interference diagram

We now turn to the final amplitude, namely that involving twice the real part of

$$= \left(-i\ \frac{g_s^2}{p_f^2}\left[\bar{u}\gamma^\mu \varepsilon^*_\mu \not{p}_f v\right]\delta_{il}t^a_{lk}\right)^*\left(-i\ \frac{g_s^2}{p_s^2 - m_a^2}\left[\bar{u}v\right]\left(p_a + p_s\right)^\nu \varepsilon^*_\nu \delta_{jk} t^a_{ij}\right) \tag{3.5.55}$$

Once again we observe the same colour factor as the above two calculations, giving the colour averaged amplitude

$$\sum_{a,i,k}\  = \frac{4g_s^4}{p_f^2(p_s^2 - m_a^2)}\left[\bar{u}\ \not{\varepsilon}^*\not{p}_f v\right]^*\left[\bar{u}v\right]\left(p_a + p_s\right)^\nu \varepsilon^*_\nu \tag{3.5.56}$$

$$= \frac{4g_s^4}{p_f^2(p_s^2 - m_a^2)}\left[\bar{v}\ \gamma^0\gamma^0\not{p}_f\gamma^0\gamma^0\not{\varepsilon}\gamma^0\gamma^0 u\right]\left[\bar{u}v\right]\left(p_a + p_s\right)^\nu \varepsilon^*_\nu \tag{3.5.57}$$

$$= \frac{4g_s^4}{p_f^2(p_s^2 - m_a^2)}\left[\bar{v}\ \not{p}_f\gamma^\mu\ u\bar{u}\ v\right]\left(p_a + p_s\right)^\nu \varepsilon^*_\nu \varepsilon_\mu \tag{3.5.58}$$

Summing over polarizations gives

$$\sum_{\varepsilon}\sum_{a,i,j}\left\langle \right| \left. \right\rangle = -\frac{4g_s^4}{p_f^2(p_s^2-m_a^2)}\left[\bar{v}\ \not{p}_f\ \gamma^\mu\ u\bar{u}\ v\right](p_a+p_s)^\mu \tag{3.5.59}$$

$$= -\frac{4g_s^4}{p_f^2(p_s^2-m_a^2)}\left[\bar{v}\ \not{p}_f\ \left(\not{p}_a+\not{p}_s\right)\ u\bar{u}\ v\right] \tag{3.5.60}$$

$$= -\frac{4g_s^4}{p_f^2(p_s^2-m_a^2)}\,\mathrm{Tr}\left[v\bar{v}\ \not{p}_f\ \left(\not{p}_a+\not{p}_s\right)\ u\bar{u}\right] \tag{3.5.61}$$

Summing over spins

$$\overline{\left\langle \right| \left. \right\rangle} = -\frac{4g_s^4}{p_f^2(p_s^2-m_a^2)}\,\mathrm{Tr}\left[\left(\not{p}_X-m_X\right)\not{p}_f\left(\not{p}_a+\not{p}_s\right)\not{p}_k\right] \tag{3.5.62}$$

$$= -\frac{4g_s^4}{p_f^2(p_s^2-m_a^2)}\,\mathrm{Tr}\left[\not{p}_X\not{p}_f\not{p}_a\not{p}_k+\not{p}_X\not{p}_f\not{p}_s\not{p}_k\right] \tag{3.5.63}$$

Using all trace and momentum relations, we arrive at

$$\overline{\left\langle \right| \left. \right\rangle} = 8g_s^4\left(\frac{2(p_a.p_k)^2}{p_a.p_j\ p_j.p_k}+\frac{2p_a.p_k}{p_j.p_k}+\frac{p_j.p_k}{p_a.p_j}-\frac{3p_a.p_k}{p_a.p_j}-\frac{m_a^2}{p_a.p_j}\right) \tag{3.5.64}$$

We now have all the ingredients necessary to compute the antenna function itself.

3.6 The antenna function

The antenna function we need to calculate is

$$a_{g/q\tilde{q}}^{\mathrm{RF}} = \frac{\left\langle \right| \left. \right\rangle + \left\langle \right| \left. \right\rangle + 2\,\mathrm{Re}\left\{\left\langle \right| \left. \right\rangle\right\}}{\left| \right|^2} \tag{3.6.1}$$

with RF meaning 'resonance-final' and $\tilde{q}$ meaning scalar quark. We will first express this in our s variables, to be followed by yet another variable change. It is easy to see that

$$\overline{\left\langle \right| \left. \right\rangle} = 16g_s^4\left(\frac{s_{ak}}{s_{aj}}-\frac{s_{jk}}{s_{aj}}-\frac{2m_a^2(s_{aj}-s_{ak})}{s_{aj}^2}\right) \tag{3.6.2}$$

$$\overline{\left\langle \right| \left. \right\rangle} = 16g_s^4\left(\frac{s_{aj}-s_{jk}}{s_{jk}}\right) \tag{3.6.3}$$

$$2\,\overline{\left\langle \right| \left. \right\rangle} = 16g_s^4\left(\frac{2s_{ak}^2}{s_{aj}s_{jk}}+\frac{s_{jk}}{s_{aj}}+\frac{2s_{ak}}{s_{jk}}-\frac{3s_{ak}}{s_{aj}}-\frac{2m_a^2}{s_{aj}}\right) \tag{3.6.4}$$

$$\overline{\left| \right|}^{\,2} = 2g_s^2 s_{AK} \tag{3.6.5}$$

We note that the interference diagram is itself real, so there is no further action to be taken in computing Eq. (3.6.1).[5] Summing Eqs. (3.6.2)-(3.6.4) and dividing by Eq. (3.6.5), we obtain

$$a_{g/q\tilde{q}}^{\mathrm{RF}} = \frac{8g_s^2}{s_{AK}}\left(\frac{2s_{ak}^2}{s_{aj}s_{jk}}+\frac{2s_{ak}}{s_{jk}}+\frac{s_{aj}}{s_{jk}}-\frac{2s_{ak}}{s_{aj}}-\frac{2m_a^2(s_{ak}-s_{jk})}{s_{aj}^2}-\frac{2m_a^2}{s_{aj}}-1\right) \tag{3.6.6}$$

[5] With the exception of computing the alternate interference diagram as a cross check, which was indeed done.

As a concluding statement we note that our antenna function is in agreement with one we have obtained using the supersymmetry model 'MSSM (ESWB)' in the automated package CalcHEP [44], which provides symbolic results for the squared matrix elements we have derived above.

3.7 Non-Dimensionalization

It is convenient to recast the antenna function using the dimensionless variables

$$y_{aj} = \frac{s_{aj}}{s_{AK} + s_{jk}}, \qquad y_{jk} = \frac{s_{jk}}{s_{AK} + s_{jk}}, \qquad \mu_a^2 = \frac{m_a^2}{s_{AK} + s_{jk}}, \qquad \mu_k^2 = \frac{m_k^2}{s_{AK} + s_{jk}} \tag{3.7.1}$$

We will see that these y variables are similar to the z variables in the parton shower and in particular when we derive the DGLAP limits that they represent Q^2. A similar definition to the above can be used for y_{ak}, but using momentum conservation we may eliminate the s_{ak} (or y_{ak}) variables. Namely, since $p_X = p_a - p_j - p_k = p_A - p_K$, we see

$$p_a^2 + p_j^2 + p_k^2 - s_{aj} - s_{ak} - s_{aj} = p_A^2 + p_K^2 - s_{AK} \tag{3.7.2}$$

$$-s_{aj} - s_{ak} + s_{jk} = s_{AK} \tag{3.7.3}$$

$$\implies s_{ak} = s_{jk} - s_{aj} - s_{AK} \tag{3.7.4}$$

Using these relations one may relegate the tedious algebra to *Mathematica* to obtain

$$a_{g/q\tilde{q}}^{\mathrm{RF}} = \frac{1}{s_{AK}} \left(\frac{2}{y_{aj} y_{jk}} + \frac{y_{aj}}{y_{jk}} - \frac{2}{y_{aj}} - \frac{2}{y_{jk}} - \frac{2\mu_a^2 (1 - y_{jk})}{y_{aj}^2} + 1 \right) \tag{3.7.5}$$

where we have now omitted the net colour and coupling factor of $8g_s^2$, i.e. to obtain the 'stripped' antenna function.

Finally, we reconstruct the mass-correction term for the b quark. The antenna function of top decay [38] contains mass corrections for initial and final state particles respectively of the form

$$\Delta m_I = \frac{-2\mu_a^2 (1 - y_{jk})}{y_{aj}^2} \tag{3.7.6}$$

$$\Delta m_F = \frac{-2\mu_k^2}{y_{jk}^2} \tag{3.7.7}$$

We see that we have the mass correction for the a particle, so inserting the k particle correction yields the final (stripped) antenna function

$$a_{g/q\tilde{q}}^{\mathrm{RF}} = \frac{1}{s_{AK}} \left(\frac{2}{y_{aj} y_{jk}} + \frac{y_{aj}}{y_{jk}} - \frac{2}{y_{aj}} - \frac{2}{y_{jk}} - \frac{2\mu_a^2 (1 - y_{jk})}{y_{aj}^2} - \frac{2\mu_k^2}{y_{jk}^2} + 1 \right) \tag{3.7.8}$$

3.8 Some Analytical Properties

3.8.1 Comparison to the Top Antenna

We note in particular the absence of a y_{jk}/y_{aj} term, such as appearing in the top decay antenna, Eq. (13) in [38]. We may examine this term to gain a physical understanding. In the rest frame of

the a particle, (and fixing the k momentum to lie on the z axis,) we evaluate

$$\frac{y_{jk}}{y_{aj}} = \frac{p_j.p_k}{p_a.p_j} \tag{3.8.1}$$

$$= \frac{(p_j)^0(p_k)^0 - \vec{p}_j.\vec{p}_k}{(m_a,\vec{0}).p_j} \tag{3.8.2}$$

$$= \frac{E_j\left(E_k - \sqrt{E_k^2 - m_k^2}\cos(\theta_{jk})\right)}{m_a E_j} \tag{3.8.3}$$

$$= \frac{E_k - \sqrt{E_k^2 - m_k^2}\cos(\theta_{jk})}{m_a} \tag{3.8.4}$$

For $m_k << E_k$ (which is not kinematically implausable) we have $\sqrt{E_k^2 - m_k^2} \approx E_k - m_k^2/2E_k$ by the binomial approximation, then

$$\frac{y_{jk}}{y_{aj}} = \frac{E_k - (E_k - \frac{m_k^2}{2E_k})\cos(\theta_{jk})}{m_a} \tag{3.8.5}$$

And therefore, ignoring terms of order m_k^2/m_a as negligible,

$$\left.\frac{y_{jk}}{y_{aj}}\right|_{\theta_{jk}\sim 0} = \frac{1}{2E_k}\frac{m_k^2}{m_a} \approx 0 \tag{3.8.6}$$

$$\left.\frac{y_{jk}}{y_{aj}}\right|_{\theta_{jk}\sim \frac{\pi}{2}} = \frac{E_k}{m_a} \tag{3.8.7}$$

$$\left.\frac{y_{jk}}{y_{aj}}\right|_{\theta_{jk}\sim \pi} = \frac{2E_k}{m_a} - \frac{1}{2E_k}\frac{m_k^2}{m_a} \approx \frac{2E_k}{m_a} \tag{3.8.8}$$

We therefore see that the absense of this term in the stop antenna results in less emission in the non-collinear direction. Indeed, as we will presently show in a special case and observe later graphically, that this difference causes quite an extreme effect in the radiation pattern at high angles to the b-quark. Incidentally, repeating this analysis easily demonstrates that the $2/y_{aj}y_{jk}$ term diverges for $E_j \to 0$ or $\theta_{jk} \to 0$, i.e. for soft or collinear emission.

3.8.2 Backwards Radiation

Let us follow the case of $\theta_{jk} = \pi/2$ to observe an interesting result. This will also shed light on the interpretation of the y variables. Consider from Eq. (3.7.4) that $s_{AK} + s_{jk} = s_{aj} + s_{ak}$ implies

$$y_{aj} = \frac{s_{aj}}{s_{AK} + s_{jk}} = \frac{s_{aj}}{s_{aj} + s_{ak}} \tag{3.8.9}$$

evaluating this in the rest frame of a gives

$$y_{aj} = \frac{2m_a E_j}{2m_a(E_j + E_k)} = \frac{E_j}{E_j + E_k} \tag{3.8.10}$$

namely, this is the energy fraction that the branched particle j takes from the parent, whose net energy is $E_j + E_k$. This is none other than the DGLAP $z = E_b/E_a$ variable we introduced in

Chapter 2.3.1. We will return to this shortly to derive the DGLAP kernel as a limit of the antenna function.
For simplicity, let us take the b quark massless. For completeness we include in Appendix D the expression for a massive quark however the conclusion will be the same. Evaluating the other variables in the same rest frame we have

$$y_{jk} = \frac{2p_j.p_k}{2m_a(E_j+E_k)} = \frac{2E_j\left(E_k - \sqrt{E_k^2 - m_k^2}\cos(\theta_{jk})\right)}{2m_a(E_j+E_k)} = \frac{4E_jE_k}{2m_a(E_j+E_k)} \tag{3.8.11}$$

$$\mu_a^2 = \frac{m_a^2}{2m_a(E_j+E_k)} = \frac{m_a}{2(E_j+E_k)} \tag{3.8.12}$$

$$\mu_k^2 = \frac{m_k^2}{2m_a(E_j+E_k)} = 0 \tag{3.8.13}$$

So the antenna function is

$$s_{AK}\ a^{\mathrm{RF}}_{g/q\tilde{q}} = \frac{m_a(E_j+E_k)^2}{E_j^2E_k} + \frac{m_a}{2E_k} - 2 - \frac{2E_k}{E_j} - \frac{m_a}{E_k} - \frac{m_a}{E_j} - \frac{m_a}{E_j} - \frac{m_aE_k}{E_j^2} - \frac{2E_k}{E_j} + 1 \tag{3.8.14}$$

$$= -1 + \frac{m_a}{2E_k} \tag{3.8.15}$$

We can solve for E_k in terms of E_j, m_a, and m_X using conservation of energy, 3-momentum, and the on-shell mass conditions

$$E_k = m_a - E_j - E_X \tag{3.8.16}$$

$$\vec{p}_X = -\vec{p}_j - \vec{p}_k \tag{3.8.17}$$

$$\implies E_X^2 = m_X^2 + (E_j+E_k)^2 \tag{3.8.18}$$

$$\implies E_k = m_a - E_j - m_X^2 + (E_j+E_k)^2 \tag{3.8.19}$$

Solving the quadratic for E_k gives

$$E_k = \frac{1}{2}\left(m_a - \frac{m_X^2}{m_a} - 2E_j\right) = \frac{m_a}{2}\left(1 - \left(\frac{m_X}{m_A}\right)^2 - \frac{2E_j}{m_a}\right) \tag{3.8.20}$$

Then the antenna function becomes

$$s_{AK}\ a^{\mathrm{RF}}_{g/q\tilde{q}} = -1 + \frac{m_a}{2}\left(\frac{2}{m_a}\frac{1}{1 - \left(\frac{m_X}{m_a}\right)^2 - \frac{2E_j}{m_a}}\right) \tag{3.8.21}$$

In our case of exact supersymmetry, we will take $m_X = m_\chi = m_W = 80.3$, the mass of the W boson and $m_a = 175$ (in units of GeV). Then for sufficiently soft gluons, $(m_X/m_a)^2 + 2E_j/m_a$ is a small quantity. Expanding to first order we have

$$s_{AK}\ a^{\mathrm{RF}}_{g/q\tilde{q}} = -1 + 1 + \left(\frac{m_X}{m_a}\right)^2 + \frac{2E_j}{m_a} = \left(\frac{m_X}{m_a}\right)^2 + \frac{2E_j}{m_a} = 0.21 + 0.01E_j \tag{3.8.22}$$

So unless the emitted gluons are very hard i.e $\mathcal{O}(m_a)$ we will have approximately no radiation in the backward direction. This particular feature of the stop antenna will be seen explicitly in Chapter 4.

3.8.3 DGLAP Kernel from the Antenna

We can obtain the DGLAP splitting kernels as limiting cases of the antenna function. Here we will reproduce the DGLAP kernel for a quark emitting a collinear gluon.
Together with the phase space, we have the probability of emission

$$a^{\mathrm{RF}}_{g/q\tilde{q}}\ \mathrm{d}\Phi_{\mathrm{ant}} = \frac{1}{4\pi s}\ C_F\ \alpha_s\ \mathrm{d}s_{aj}\mathrm{d}s_{jk}\frac{\mathrm{d}\phi}{2\pi}\ a^{\mathrm{RF}}_{g/q\tilde{q}} \tag{3.8.23}$$

where C_F is a colour factor. From here we will suppress the $\mathrm{d}\phi$ measure (or equivalently integrate it since it is normalized), and we have substituted $g_s^2 = 4\pi\alpha_s$ into our antenna function to match with the DGLAP phase space. The limits of collinear radiation are characterised by $y_{jk} \to 0$ and $y_{aj} \to 0$:

$$y_{aj} = \frac{p_a.p_j}{p_a.p_j + p_a.p_k} = \frac{E_a E_j(1-\cos(\theta_{aj}))}{p_a.p_j + p_a.p_k} \underset{\theta_{aj}\to 0}{\longrightarrow} 0 \tag{3.8.24}$$

$$y_{jk} = \frac{p_j.p_k}{p_a.p_j + p_a.p_k} = \frac{E_j E_k(1-\cos(\theta_{jk}))}{p_a.p_j + p_a.p_k} \underset{\theta_{jk}\to 0}{\longrightarrow} 0 \tag{3.8.25}$$

We will demnonstrate here the $y_{jk} \to 0$ case. First, recall our definition of the energy fraction $z = E_b/E_a$. In this expression E_a is the total energy available to the parent before the branching, and E_b is the energy of the daughter b. So, identifying the appropriate variables ($b = j$, $c = k$), we evaluate the y's in the rest frame of a:

$$y_{aj} = \frac{m_a E_j}{m_a(E_j + E_k)} = z \tag{3.8.26}$$

$$y_{jk} = \frac{m_a E_k}{m_a(E_j + E_k)} = 1 - z \tag{3.8.27}$$

where we understand that $E_a = E_j + E_k$. Next, using $s = s_{AK} + s_{jk}$

$$a^{\mathrm{RF}}_{g/q\tilde{q}}\ \mathrm{d}\Phi_{\mathrm{ant}} = \frac{1}{4\pi}C_F\alpha_s\frac{\mathrm{d}s_{aj}}{s_{AK}+s_{jk}}\ \frac{\mathrm{d}s_{jk}}{s_{AK}+s_{jk}}(s_{AK}+s_{jk})\ \frac{1}{s_{AK}}\left(s_{AK}a^{\mathrm{RF}}_{g/q\tilde{q}}\right) \tag{3.8.28}$$

$$= \frac{1}{4\pi}C_F\alpha_s\ \mathrm{d}y_{aj}\ \mathrm{d}y_{jk}\ \frac{1}{y_{AK}}\left(s_{AK}a^{\mathrm{RF}}_{g/q\tilde{q}}\right) \tag{3.8.29}$$

We have, therefore

$$a^{\mathrm{RF}}_{g/q\tilde{q}}\ \mathrm{d}\Phi_{\mathrm{ant}} \underset{\theta_{jk}\to 0}{\longrightarrow} \frac{1}{4\pi}C_F\alpha_s\ \mathrm{d}y_{aj}\ \frac{\mathrm{d}y_{jk}}{y_{jk}}\frac{y_{jk}}{y_{AK}}\left(s_{AK}a^{\mathrm{RF}}_{g/q\tilde{q}}\right) \tag{3.8.30}$$

$$= \frac{1}{4\pi}C_F\alpha_s\ \mathrm{d}y_{aj}\ \frac{\mathrm{d}y_{jk}}{y_{jk}}\frac{y_{jk}}{y_{AK}}\left(\frac{2}{y_{aj}y_{jk}} + \frac{y_{aj}}{y_{jk}} - \frac{2}{y_{jk}} - \frac{2\mu_k^2}{y_{jk}^2}\right) \tag{3.8.31}$$

where we have dropped all terms nonsingular in y_{jk}. Expanding and using $y_{jk} + y_{AK} = 1$,

$$= \frac{1}{4\pi}C_F\alpha_s\ \mathrm{d}y_{aj}\ \frac{\mathrm{d}y_{jk}}{y_{jk}}\frac{1}{1-y_{jk}}\left(\frac{2}{y_{aj}} + \frac{y_{aj}}{1} - 2 - \frac{2\mu_k^2}{y_{jk}}\right) \tag{3.8.32}$$

$$= \frac{1}{4\pi}C_F\alpha_s\ \mathrm{d}y_{aj}\ \mathrm{d}\ln(y_{jk})\frac{1}{1}\left(\frac{1}{z} + z - 2 - \frac{2\mu_k^2}{y_{jk}}\right) \tag{3.8.33}$$

Note here that the term $2\mu_k^2/y_{jk}$ is nonsingular in $y_{jk} \to 0$. This is consistent with the definition of the quasi-collinear limit [37], however for direct comparison with the DGLAP kernels in Appendix A we will take $m_k = 0$ as well. Our expression reduces to

$$a_{g/q\tilde{q}}^{\mathrm{RF}}\ \mathrm{d}\Phi_{\mathrm{ant}} \to \frac{1}{4\pi} C_F \alpha_s\ \mathrm{d}y_{aj}\ \mathrm{d}\ln(y_{jk}) \left(\frac{1+z^2-2z}{z}\right) \tag{3.8.34}$$

from which we can identify $\mathrm{d}t = \mathrm{d}\ln(y_{jk})$ and $\mathrm{d}z = \mathrm{d}y_{aj}$, and we recover the splitting kernel

$$P_{q\to qg}(z) = \frac{1-2z+z^2}{z} = \frac{(1-z)^2}{z} \tag{3.8.35}$$

which is in agreement with the known DGLAP kernel for gluon emission off a quark. Thus we have proven that the parton shower is indeed, a limiting case of the antenna shower.

3.8.4 Helicity decomposition

We note that it is possible to recover the individual helicity contributions to the antenna function. Denoting helicities with a + for positive helicity, − for negative, or 0 for the spin-0 particle, then in the Born level the only helicity conserving processes are

1. $0 \longrightarrow ++$ (i.e. helicity 0 stop decays to positive helicity bottom and chargino)
2. $0 \longrightarrow --$

To understand this, note that the decay in position space may be represented as

$$\longleftarrow \cdot \longrightarrow$$

where the dot is the stop quark and the arrows are the momenta of the daughter partons. The only way this decay can conserve the helicity of the stop, i.e. 0, is if the daughters have the same helicity. In the Born+1 case these become:

1. $++ \longrightarrow +++$ or $++ \longrightarrow ++-$
2. $-- \longrightarrow --+$ or $-- \longrightarrow ---$

where the final symbol represents the gluon helicity. Since the amplitude for a scalar to decay into either two positive or negative helicity fermions is necessarily symmetric, we will simply work with the $0 \longrightarrow ++$ processes. From [13], we have the individual DGLAP kernels for the emission of a + or − gluon from a + quark:

$$P_+(z) = \frac{1}{z} \tag{3.8.36}$$

$$P_-(z) = \frac{(1-z)^2}{z} \tag{3.8.37}$$

It is easy to see that these add to give (3.8.35). Using these, one can now reverse-engineer the DGLAP limits of the antenna into the respective helicity contributions. For instance we see that

$$a_{+-} \sim \frac{1}{y_{jk}} P_- = \frac{1}{y_{jk}} \frac{(1-z)^2}{z} \tag{3.8.38}$$

$$= \frac{1}{y_{jk}} \frac{(1-y_{aj})^2}{y_{aj}} \tag{3.8.39}$$

$$= \frac{1}{y_{jk} y_{aj}} - \frac{2}{y_{jk}} + \frac{y_{aj}}{y_{jk}} \tag{3.8.40}$$

So the $+-$ part of the antenna function contains the above, plus some term nonsingular in $y_{jk} \to 0$. By the same reasoning for the $-$ helicity gluon we obtain

$$\bar{a}_{+-} = \frac{1}{y_{jk}y_{aj}} - \frac{2}{y_{jk}} + \frac{y_{aj}}{y_{jk}} + A \tag{3.8.41}$$

$$\bar{a}_{++} = \frac{1}{y_{jk}y_{aj}} + B \tag{3.8.42}$$

where we have defined $\bar{a} = s_{AK}\ a$. Observe here how the eikonal factor arises due to soft gluon emission of either helicity. This helicity independence explains why the universal structure of the eikonal contains a factor of 2. Now, summing and averaging over helicities and using the symmetry noted above, $a = (\bar{a}_{+-} + \bar{a}_{++})$ which constrains

$$B = 1 + \frac{2\mu_a^2(y_{jk} - 1)}{y_{aj}^2} - \frac{2}{y_{aj}} - A \tag{3.8.43}$$

One could then also obtain the collinear limit of emission from the stop quark. Using the symmetry of emitting a $+$ or $-$ helicity gluon from a scalar, one obtains the corresponding a_{++}, a_{+-} terms by halving the limits of the antenna. Comparing with the previous results, then, one could obtain an expression for A and thus obtain a complete decomposition in helicities. Regrettably, this analytical work has not yet been concluded and we defer this to a later study.

3.9 Further Antennae

Since we aim to simulate radiative corrections in a stop-decay event, we must realize that there are several possible antennae that we may find. These are shown in Figure 3.6.

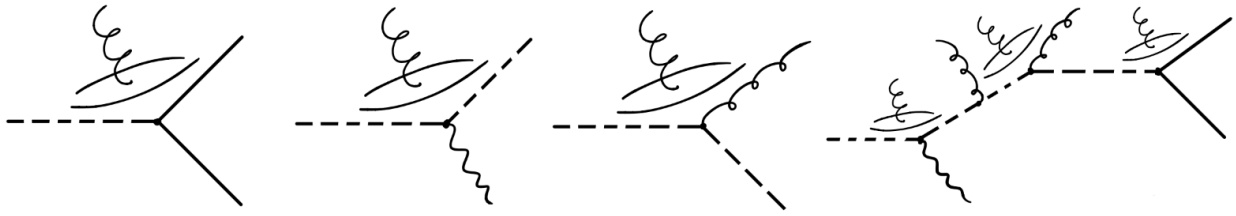

Figure 3.6: First on the left is the squark-quark (SQ) antenna. Second the stop-stop (SS) antenna. Third the stop-gluon (SG) antenna. Fourth an example of a branching containing dipoles of all types. We note that the SS antenna is not possible according to our toy Lagrangian but may occur within the context of a full BSM event generator.

We can justify the form of each antenna by our knowledge of the universal terms that appear. We know already the SQ antenna. As we have noted, the difference between the SQ and QQ antennae is the absence of a y_{jk}/y_{aj} term. We interpret this as a spin depenent collinear pole, since it is singular for gluon emission collinear to the a particle and is absent when a is a scalar. The SS antenna we may then write

$$a_{g/\tilde{q}\tilde{q}}^{RF} = \frac{1}{s_{AK}}\left(\frac{2}{y_{aj}y_{jk}} - \frac{2}{y_{aj}} - \frac{2}{y_{jk}} - \frac{2\mu_a^2(1 - y_{jk})}{y_{aj}^2} - \frac{2\mu_k^2}{y_{jk}^2} + 1\right) \tag{3.9.1}$$

Next, consider the QG-IF type antenna, namely Eq. (23) in [16]. It is a simple matter of algebra to observe that their result contains the same terms as above, with the addition of y_{aj}/y_{jk} and y_{jk}/y_{aj} terms, and a novel $-y_{aj}^2/((1-y_{jk})y_{jk})$. Applying the same logic in reducing this to a stop-gluon antenna, we can obtain our antenna function as

$$a_{g/g\tilde{q}}^{RF} = \frac{1}{s_{AK}}\left(\frac{2}{y_{aj}y_{jk}} - \frac{2}{y_{aj}} - \frac{2}{y_{jk}} - \frac{2\mu_a^2(1-y_{jk})}{y_{aj}^2} - \frac{y_{aj}^2}{(1-y_{jk})y_{jk}}\right) \tag{3.9.2}$$

Chapter 4

VINCIA Implementation

In this section and the next we will present the results of our numerical studies. First we will show the radiation pattern in an isolated $\tilde{t} \to b\tilde{\chi}$ decay with some comparisons to various other results, and then we will investigate the outcome of the fully-fledged event generation in Pythia.

4.1 Standalone Antenna Functions

We will plot the value of $s_{AK}\ a^{\mathrm{RF}}_{g/q\tilde{q}}$ on a logarithmic scale as a function of the angle θ_{jk} between the gluon and the b quark, evaluated in the rest frame of the stop quark. Since we will vary the energy of emitted gluons, we require a relation between E_k, E_j and the known masses of the other particles. We have given hints of how these calculations should be done in Chapter 3.8.2 and in general the same is done here, however relating E_k to E_j is a nontrivial matter and a full derivation is given in Appendix E.

In Figure 4.1 we plot the antenna function for stop decay. In the left plot we use $m_{\tilde{t}} = 175$, $m_b = 4.5$, $m_{\tilde{\chi}} = 80.3$ in units of GeV. We observe immediately several properties of the radiation. Firstly the probability of emission for soft gluons is logarithmically enhanced; everywhere except in the backward direction, soft radiation is orders of magnitude more probable than hard radiation. Likewise, in the close-to-collinear region we see further enhancement for all gluon energies. These are simply artefacts of the universal soft and collinear singularities of QCD.

However in the exactly collinear limit we observe a suppression in the radiation pattern up to some opening angle θ_{dead}, well known in the literature as the dead cone effect [45, 46], whereby collinear emission is kinematically suppressed, since a massive parton cannot emit massless gluons collinearly. For comparison, we have shown in the other plot the same antenna pattern but with a massless b quark. We observe how the collinear limit is vastly enhanced.

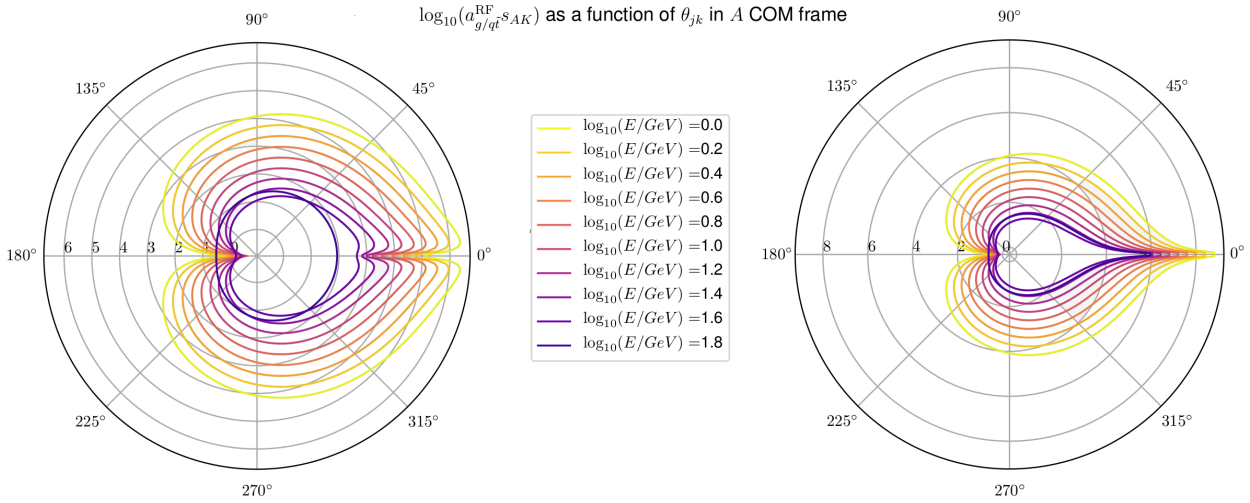

Figure 4.1: A plot of the log of the radiation pattern in polar coordinates. The value of the antenna function for curves of constant gluon energy (shown in the legend) is the radial coordinate and the antenna function is evaluated in the rest frame of the top quark, the angle is the angle of the emitted gluon with respect to the b quark. The left plot uses a b quark mass of 4.5 GeV, the right uses 0.01 GeV.

We see also that radiation grows more and more suppressed with the angle of emission, and as shown analytically, reaching an extreme in the exactly anticollinear direction with approximately zero radiation. This is a consequnce of the interference effects that the antenna function captures, as we will see when we compare with the equivalent DGLAP splitting kernel.

Before we do this, note however that we are in the rest frame of the stop quark. So consider again the Born+1 amplitude for when the gluon is emitted form the stop quark, Fig. 3.4. It contains a factor $\varepsilon_\mu(q)(p_a + p_s)^\mu = \varepsilon_\mu(2p_a - q)^\mu = 2p_a.\varepsilon(q)$ where q^μ is the 4-momentum of the gluon and we have used the Lorenz gauge condition $q.\varepsilon(q) = 0$ in the last equality. Since we are in the rest frame of a, this reduces to $m_a\varepsilon_0(q)$, however in the Lorenz gauge ε is a timelike vector, so $m_a\varepsilon_0(q) = 0$. Namely, in the rest frame, the stop quark cannot radiate. This is no surprise: a particle at rest does not radiate. It is therefore an interesting observation that in the rest frame, all dynamics, including interference effects, are contained solely in the diagram where gluons are emitted from the bottom quark. From this we see that even in a frame where there can be no interference between the two ends of the dipole (i.e. since one end is not radiating), emission from one end is nonetheless influenced by the other. We will turn to this again when we compare the antenna patterns of the top to the stop.

First, we compare the antenna function to the equivalent DGLAP kernel. In Figure 4.2 we display the equivalent plots as above: on the left the log of the DGLAP kernel, and on the right the fraction of the antenna function that it reproduces. We observe good agreement up to an emission angle $\sim 30°$, however the DGLAP kernel rapidly loses information beyond this. This of course is since the DGLAP kernels are derived in the collinear limit. We see this assmuption begins to break down at $\sim 30°$.

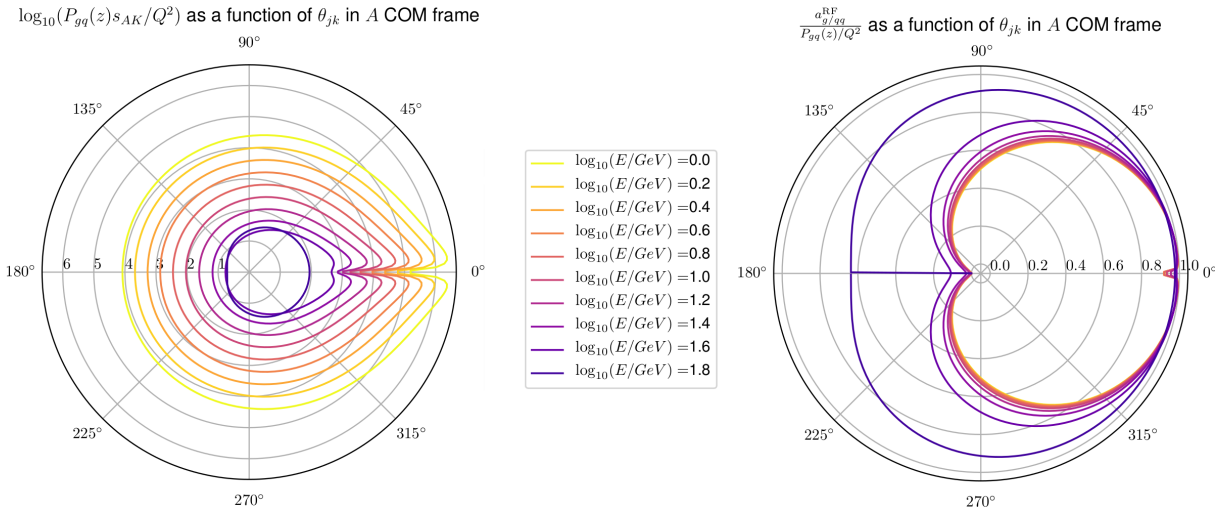

Figure 4.2: The DGLAP splitting kernel on the left with the ratio of antenna to DGLAP on the right.

Finally we look at the consequences of spin on the radiation pattern. In Figure 4.3 we plot the ratio of the antenna function for $\tilde{t} \to bg\tilde{\chi}$ to $t \to bgW$, where we have used the antenna function for top decay from [38]. We observe, as expected, agreement in the collinear limit, and in the soft limit. Of course, our gluons are not infinitely soft so the agreement is only approximate, but very good at almost all angles. We see that for all angles and for a vast range of gluon energies, $a^{\mathrm{RF}}_{g/b\tilde{t}} \leq a^{\mathrm{RF}}_{g/bt}$, and in particular the stop antenna is far more suppressed at high angles. We conclude that the stop is more sensitive to destructive interference, and that the top antenna is able to radiate anticollinear to the b quark.

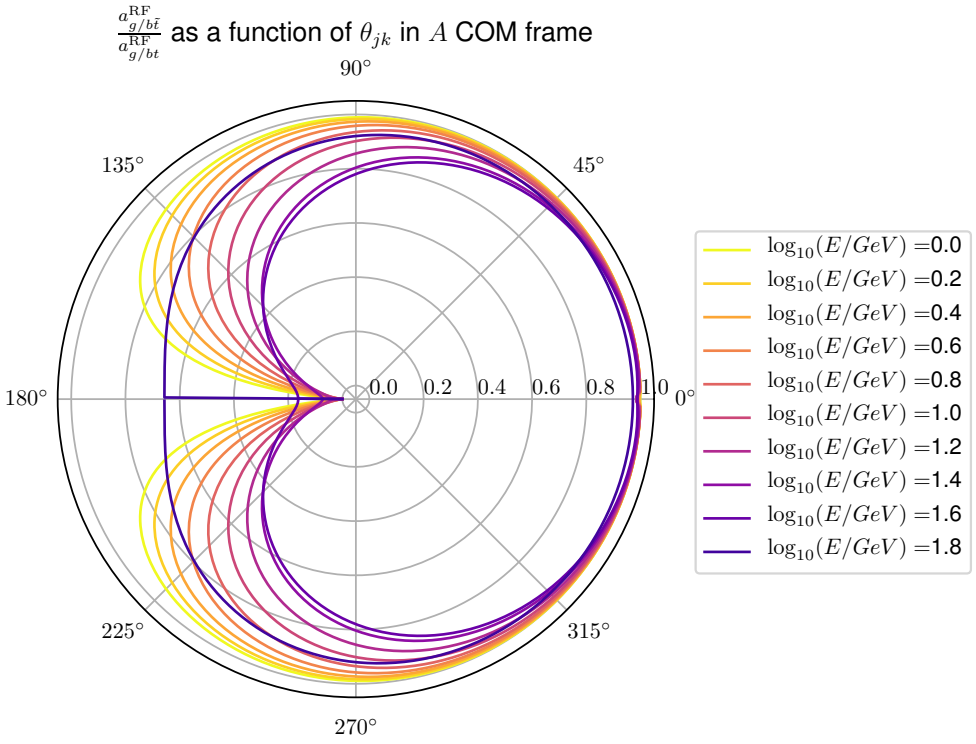

Figure 4.3: The ratio of the stop to the top antenna.

Chapter 5

Event Generation

The above have been simply the radiation patterns for emission of an isolated $\tilde{t}b$ antenna. To study realistic events, we embed our RF antennae as C++ functions within the Vincia shower framework. We study an e^+e^- collision where unless specified, the center of mass energy has been taken as 500 GeV. The e^+e^- annihilate to produce some general resonance R which is then forced to decay into either a stop-antistop or top-antitop pair. Thus the two processes we study are essentially $t\bar{t} \to bW^+\bar{b}W^-$ and $\tilde{t}\tilde{t}^* \to b\tilde{\chi}^+\bar{b}\tilde{\chi}^-$, where $\tilde{t}^*$ is the antistop quark. We will refer to the top/stop as the resonance. We force the chargino and the W boson stable to study the stop antenna in isolation, and set the width of the stop the same as that of the top. We have not at this stage activated hadronization, however for a realistic analysis this, and W decay, will be necessary, and is deferred to a later investigation.

To study the events we require an infrared (IR) and collinear safe (IRC safe) variable [15], namely, an observable that is physically meaningful and measurable. The IRC variables are invariant under the addition of either: any number of infinitely soft gluons; or an exactly collinear gluon. For example, if we consider the number of gluons emitted in an annulus around the b-quark, two exactly collinear gluons would be counted as two separate gluons, whereas in reality a detector may only be able to resolve one single gluon with twice the energy and momentum of the separate gluons. Instead we have studied the energy density of gluons in such an annulus. The emission of a collinear gluon or an infinitely soft gluon does not change the value, hence this is a suitable variable to study.

5.1 Monte Carlo Results

In Figure 5.1 we present a statistical average of the gluon angular energy density as a function of angle with respect to the b quark. We use the same labelling as before, with a, j, k referring to the (s)top, gluon, bottom respectively. We define the lab frame as the center of mass frame of the e^+e^- system. In this frame we see that emission is highly collinearly enhanced and drops rapidly beyond 10°, before reaching a local maximum at ∼140° for top and stop events. We will study this behaviour by boosting to the rest frame of the a particle, so that our radiation patterns of Chapter 4 are of direct use: these are the dashed lines.

We observe that the energy spectrum in a stop event is lower than in a top event for all angles. Except for the collinearly enhanced region, which our previous arguments of universality suggest must agree, we observe some interesting properties which we shall discuss before turning to the discrepancy in the collinear region.

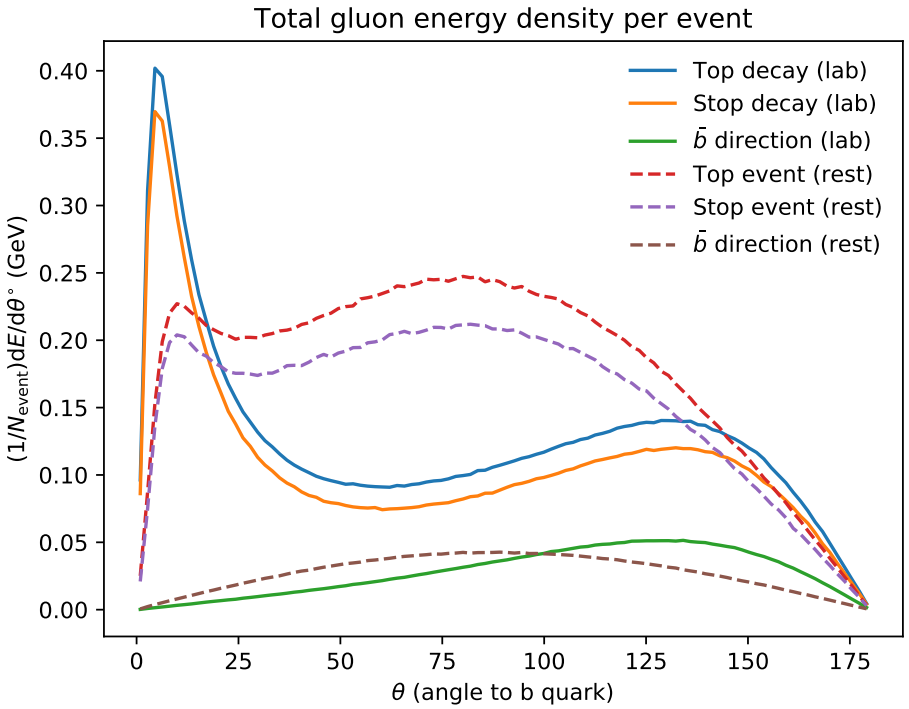

Figure 5.1: The total gluon energy density per event plotted in both the lab and rest frame. The solid lines show the value of the observable in the center of mass frame of the collision, while the dashed lines are in the rest (center of mass) frame of the top/stop.

Considering now the second peak in the plot, we see this is present due to the other branch of the decay, involving the anti-b quarks. With the brown dashed line we have shown the distribution of the $\bar{b}$ direction with respect to the b. We know by charge conjugation symmetry that a $\tilde{t}^* \to \bar{b}\tilde{\chi}^-$ process will have the same antenna function, and therefore the same collinear enhancement. This peak corresponds exactly with the peak of the $\bar{b}$ direction, as expected. A natural question is then: if there is a radiating b quark here, why is there no obvious evidence of a dead cone as a dip in the energy density here?
Firstly, the $\bar{b}$ direction is distributed as shown in the plot. For each event there will of course be some dead cone but upon averaging over a large number of events, these dead cones will be 'filled in' by the contributions of other events. However, we note that there in fact *is* a small dip in the gluon energy density at precisely the peak location of the $\bar{b}$ direction. It is tempting to attribute small variations in the slope of the plot to statistical fluctuations, however Figure 5.1 is an average over 5 million events, and random deviations will have largely been suppressed. On careful scrutiny, there are several dips that do not correspond to the peak $\bar{b}$ direction, and therefore are likely to indicate the directions of other radiating particles. We note in particular the approximately constant difference in the two energy distributions between 50° and 130°. This is not something that one would not expect from a naïve investigation of the standalone antenna pattern. It is possible that the other radiating particles are spread out in such a way that their cumulative radiation patterns average out over many events to create this constant difference.

Now let us turn again to the discrepancy in the collinear limit. From the figure above, we estimate a difference of 0.02 GeV per degree. We investigate the possibilities of this being caused by: trivial differences due to different colour factors of the antennae; uncertainties due to the process-dependent nonsingular terms that the antenna functions for each process may have; radiation from the anti(s)top quarks contaminating the region collinear to the b; or radiation from the $\bar{b}$ quark producing contamination. To test the first three hypotheses we plot, in order: the same event but with all colour factors forced to 3;[1] the antenna functions with an additive $+2+2\mu_k^2/y_{jk}$; the event at the production threshold of $E_{cm} = 350$ GeV; and a decomposition of the spectrum, showing gluons that have the b quark as an ancestor, and those that do not. These can be found in Figures 5.2-5.5.

Examing these plots we conclude that the issue of the collinear discrepancy can be attributed to many factors. Firstly note that the stop/top ratio of Figure 4.3 shows that from 90° onward, the stop antenna begins radiating appreciably less than the top antenna. Therefore it is physically plausible that the collinear peaks do not agree and that the top peak is larger since there is more contamination from high-angle radiation of the $\bar{t}\bar{b}$ antenna than the $\tilde{t}^*\bar{b}$ one (however as we will see when we turn to the dead cone, this effect is not as pronounced as one would expect based the stop/top ratio alone).

While the deviation is not entirely removed in any of these figures, we nonetheless observe an improvement in most. The deviation is ultimately on the order of 0.01 GeV which upon closer inspection of the stop/top ratio plot, could be explained by the small deviations in the radiation pattern. Now, since the antenna captures radiation rates it does not necessarily have a one to one correspondence with the energy density plots, so analyzing an event using only the antenna pattern is bound to eventually lead to inaccuracies. Having understood this however, since the ratio of stop/top begins deviating slightly from unity at small angles, perhaps our result is not entirely unexpected. As a final point, we have seen by varying the colour factors that, while the antennae themselves are universal, a process-dependence in this particular variable may be introduced by the statistics, rather than the kinematics.

[1] We use an input Vincia:*AntennaClass*:chargeFactor = 3.0 to the .cmnd file of the Pythia script, where the AntennaClass is a class within C++ containing the antenna functions we have implemented

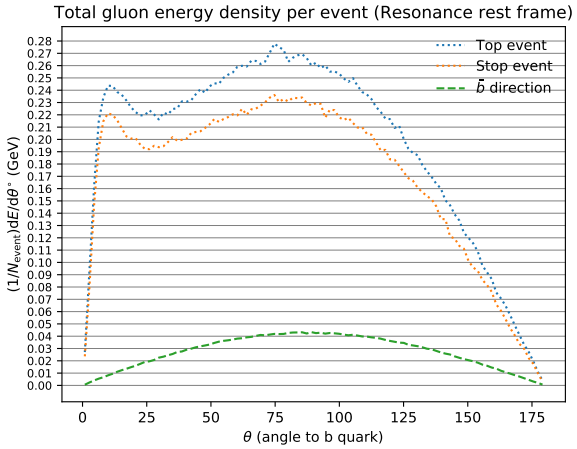

Figure 5.2: Gluon energy density in the resonance rest frame, with all colour factors set to 3. We observe the same general shape, with a peak difference in the collinear region approximately 0.02 GeV.

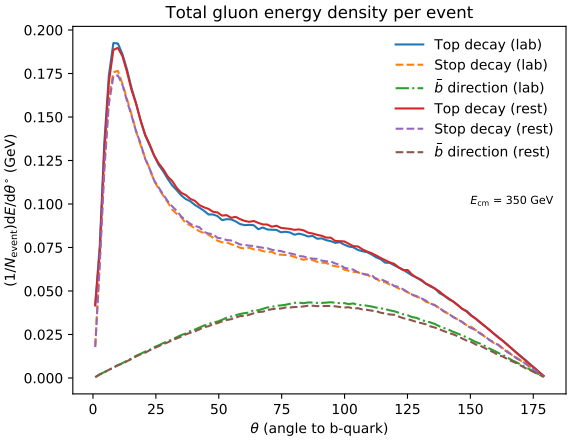

Figure 5.3: Energy density at production threshold $E_{cm} = 350$ GeV in the lab and rest frames. These are similar, as expected since the resonance is produced at rest. Boosting into the top rest frame gives the anti-top some backward velocity, slightly shifting the energy spectrum toward higher angls. We observe a collinear difference approximately 0.01 GeV.

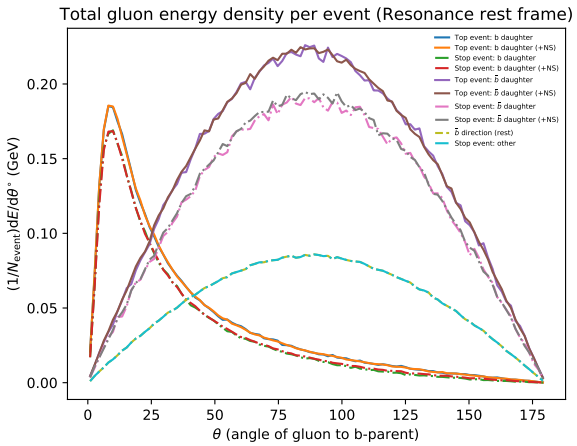

Figure 5.4: Energy density with and without nonsingular terms. Small differences are visible but negligible. Shown in the legend is $(+NS)$ meaning 'plus non-singular.' The solid and dash-dotted lines respectively pertain to Top and Stop events

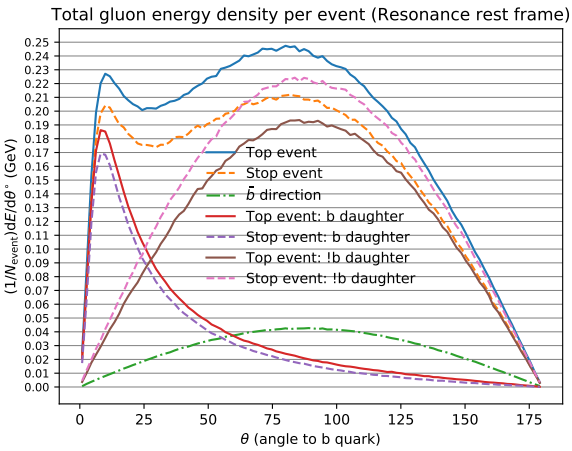

Figure 5.5: We plot the gluons that have either the b quark as an ancestor, with the lines labelled 'b daughter,' or that do not have the b as an ancestor, with '!b daughter'. Once again the collinear discrepancy is not eliminated but reduced to approximately 0.015 GeV.

5.2 Heavy Stop Quark

To probe the dependence of our results on the mass of the stop quark, we simulate a hypothetical e^+e^- collision at 3 TeV with a stop mass of 1000 GeV. In Figure 5.6 we observe that in the rest frame of the (s)top, the radiation pattern is highly collimated. This is due to the mass of the b quark being negligible compared to the now heavy stop quark. Consequently the dead cone effect is bypassed and the b can radiate profusely in the collinear direction.

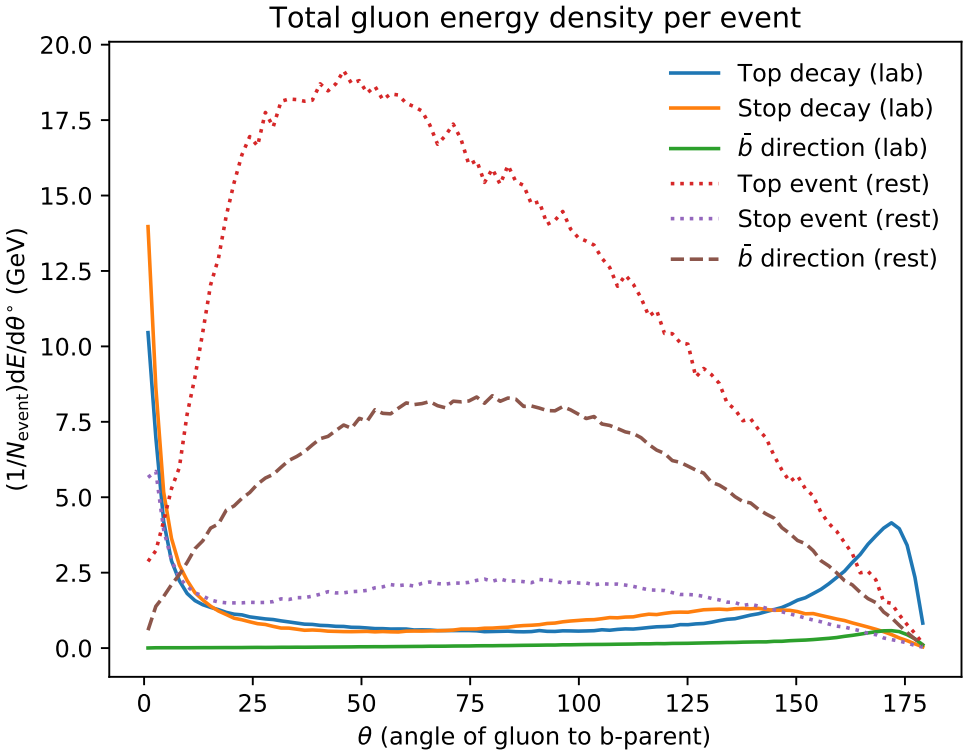

Figure 5.6: (S)top decay at 3 TeV with $m_{\tilde{t}} = 1000$ GeV, $m_t = 175$ GeV, $m_b = 4.5$ GeV, $m_\chi = 80.3$ GeV. Note that the normalization of the b and $\bar{b}$ lines is rather meaningless here; the area beneath the curves must be 1 but in order for the peaks to be discernable we have had to manually scale the output.

5.3 Dead Cone Studies

Finally we study the effect of varying the b mass on the dead cone. As we have mentioned, the dead cone is a kinematical consequence of radiation from massive particles. If a quark of mass m and energy E is radiating, then the dead cone angle will be [46] of the order of $\theta_{\text{dead}} \sim m/E$. We show in Figure 5.7 the gluon energy distribution for a range of b masses. We observe in the massive case that the expected collinear enhancement is almost entirely suppressed so that the consequent radiation pattern is quite uniformly distributed. We observe a very strong dependence of the collinear zone on the b mass. We go from almost no energy in the forward direction at $m_b = 6$ to a very large and relatively sharp peak at $m_b = 0.1$ GeV.
We observe that the dead cone angle as seen in the plots only matches the value of m/E to order magnitude. For example if $m_b = 6$, $m/E = 6.6^\circ$ but the plot suggests $\theta_{\text{dead}} \approx 10^\circ$. In Ref. [45] the

dead cone angle is derived not as an explicit relation but rather that emission is supressed up to small angles order of m/E. We have been unable to find a more detailed study between the dead cone angle and the ratio m/E in the literature, but we seem to nonetheless agree with the expected result to within a factor of 2.
Finally it is worth nothing that at $m_b = 4.5$, the mass used for all results in the previous section, the energy spectrum is quite uniform, so that in the events we have examined, the contamination into, for example, the collinear region due to the $\bar{b}$, is quite uniform as well. For this reason the high angle contamination from the $\bar{b}$, as discussed in Section 5.1, does not behave in the same way as the antenna pattern would suggest.

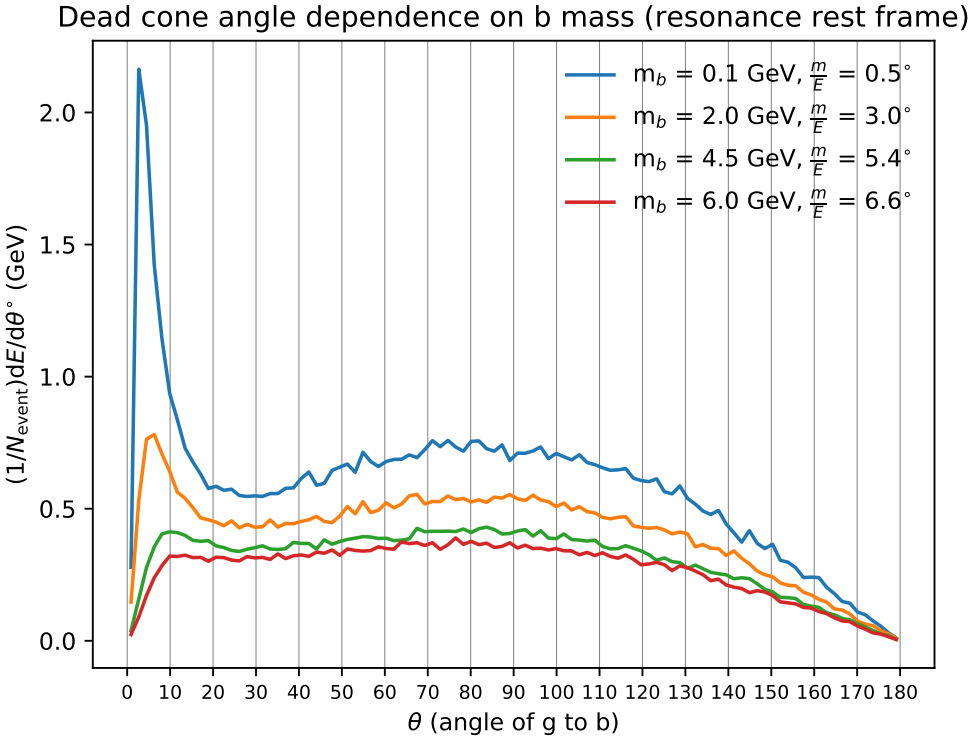

Figure 5.7: The gluon energy distribution for b quarks of varying mass, with the average values of m/E over all events included in the legend.

Chapter 6

Final Remarks

In this thesis we have introduced the parton and antenna showers as highly versatile and successful theoretical tools to not only test the existing physics in the Standard Model, but to understand the predictions of possible BSM models. We have outlined the theoretical and algorithmic basis on which they are formulated and reviewed some of the limitations of the parton shower formalism, namely the inexact treatment of coherent radiation. We have presented the antenna formalism as a step up from the parton shower, where instead of independently radiating (colour) monopoles one considers independently radiating (colour) dipoles, and outlined some recent studies of resonance decays.

Having derived an antenna function for stop decay, we compared the radiation pattern of a stop-bottom dipole to the top-bottom dipole which was investigated under the antenna formalism by Brooks and Skands [38]. As a preliminary investigation, we have worked in an exactly supersymmetric limit, where the properties of the superpartners match exactly those of their SM counterparts, so that we study in isolation the impact of the spin structure of some particle event on the radiation pattern, without the overcomplication of some possibly unknown BSM physics.

We have concluded, by considering the radiation pattern plotted in the rest frame of the stop quark, for a stop and top mass of 175 GeV, bottom mass 4.5 GeV and W and chargino mass 80.3 GeV, that the coherent decay of the stop quark is more sensitive to destructive interference than its top counterpart. While the top and the stop antennae agreed in the limit of gluon emission collinear to the bottom quark, the stop antenna began to diminish from an angle of 45° onward. Unique to the decay of our spin-0 particle, we showed that the radiation 180° from the b-quark was approximately zero. Furthermore, due to the well known dead cone effect, there is a suppression of radiation in the forward direction, however this is a property of the b quark, not the resonance and therefore is present in both the top and stop antennae.

Upon understanding the radiation pattern of a single stop-bottom dipole we have implemented our antenna functions into *C++* classes within the Vincia shower, however neglecting hadronization effects. We found that the energy spectrum of the stop was always smaller than that of the top, even in the collinear region where we expect agreement. The discrepancy of approximately 0.02 GeV per degree was attributable to a number of factors, primarily the different colour-counting statistics of different events, and the suppression of high angle emission from the anti-bottom quark in the stop antenna giving rise to a smaller amount of contamination collinear to the b.

Finally we studied the well known dead-cone effect of QCD via the dependence of the angular distribution of gluons on the mass of the bottom quark. While for $m_b = 6$ GeV the radiation in the collinear direction was heavily suppressed, providing an approximately uniform energy spectrum at all angles, a very light, $m_b = 0.1$ b featured very strongly enhanced emissions in the collinear direction. The dead cone angle is cited in the literature as $\theta_{\text{dead}} \sim m_b/E_b$, and we find that our

value of m_b/E_b and the observed dead cone agrees up to the expected order of magnitude.
Ours has only been a preliminary study into the dependence of radiation on the spin structure of an event. Even to this end there is further work: a supersymmetric theory may also contain spin-1/2 colour-octets, known as gluinos, whose radiation patterns would likely prove interesting compared to gluon and quark patterns. We have only studied events in the specialized context of no W or chargino decays, and no hadronization. In any realistic simulation, we must include both these contributions.
In general we have demonstrated the properties of the antenna shower, and due to the nature of our study, in particular and lack of evidence for SUSY at the LHC, we are unable to test the validity of our model through experimental comparisons. We have, however, made comparisons to highlight the quantitative and qualitative differences arising from spin-0 decay instead of spin-1/2 decay, and we hope that our antenna shower can be used to generate more accurate simulations in fully-fledged studies of supersymmetry in the future.

Appendix A

DGLAP splitting kernels

If $P_{a\to bc}(z)$ is the tree level splitting kernel for the process $a \to bc$ and $z = E_b/E_a$, we have [21]

$$P_{q\to qg}(z) = C_F \left[\frac{1+z^2}{1-z}\right] \tag{A.0.1}$$

$$P_{g\to gg}(z) = C_A \left[\frac{1-z}{z} + \frac{z}{1-z} + z(1-z)\right] \tag{A.0.2}$$

$$P_{g\to q\bar{q}}(z) = T_R \left[z^2 + (1-z)^2\right] \tag{A.0.3}$$

where

$$T_R = \frac{\mathrm{Tr}\,(t^a t^a)}{8} = \frac{1}{2} \tag{A.0.4}$$

$$C_A = 3 \tag{A.0.5}$$

$$C_F = \frac{\mathrm{Tr}\,(t^a t^a)}{3} = \frac{4}{3} \tag{A.0.6}$$

These are the so called 'unregularized' splitting kernels, however further details are beyond the scope of this thesis. Furthermore the phase space factorizes as

$$\mathrm{d}\Phi_{n+1} = \mathrm{d}\Phi_n \frac{1}{4(2\pi)^3} \mathrm{d}t \frac{\mathrm{d}z}{z} \mathrm{d}\phi \tag{A.0.7}$$

with $t = (p_b + p_c)^2 = 2E_bE_c(1-\cos\theta_{bc}) \approx E_bE_c\theta_{bc}^2$.

Appendix B

Sudakov Veto Algorithm

We wish to prove that using an overestimate on the sudakov factor, so that we solve

$$\ln R = -\int_t^{t_0} A(t') + B(t')\ dt' \tag{B.0.1}$$

for t with a probability of acceptance $P_A = \dfrac{A}{A+B}$ gives us the same distribution of splitting times t as solving the original Sudakov factor

$$\ln R = \exp\left(-\int_t^{t_0} A(t')\ dt'\right) \tag{B.0.2}$$

would. Let us then obtain an expression for the probability to generate a trial at time t. Let

$$\hat{\Delta}(t_a, t_b) = \exp\left(-\int_{t_a}^{t_b} A + B\ dt\right) \tag{B.0.3}$$

be the overestimated Sudakov factor, where in particular we define the probability of a splitting event to occur at time t as $A(t) + B(t)$, and let

$$\Delta(t_a, t_b) = \exp\left(-\int_{t_a}^{t_b} A\ dt\right) \tag{B.0.4}$$

be the original Sudakov factor. Then consider the case where there have been no rejected trials between times t_0 and t. The probability P_0 then, to accept a trial at time t is

$$P_0 = \underbrace{\hat{\Delta}(t_0, t)}_{\Pr(\text{no emit})}\ \underbrace{A(t)/(A(t)+B(t))}_{\Pr(\text{accept})}\ \underbrace{(A(t)+B(t))}_{\Pr(\text{Event})} \tag{B.0.5}$$

$$= \hat{\Delta}(t_0, t)A(t) \tag{B.0.6}$$

However we also have the possibility of rejecting an event at time t_1 (i.e. t_1 integrated over), so that the probability P_{10} to accept a trial at time t with either no rejections or one rejection is

$$P_{10} = P_0 + \int_{t_0}^{t} \mathrm{d}t_1\ \hat{\Delta}(t_0, t_1)\frac{B(t_1)}{A+B}\,(A+B)\,\hat{\Delta}(t_1, t)\frac{A(t)}{A+B}\,(A+B) \tag{B.0.7}$$

$$= \hat{\Delta}(t_0, t)A(t) + A(t)\int_{t_0}^{t} \mathrm{d}t_1\ \hat{\Delta}(t_0, t_1)\hat{\Delta}(t_1, t)B(t_1) \tag{B.0.8}$$

Now observe that

$$\hat{\Delta}(t_0,t_1)\hat{\Delta}(t_1,t) = \exp\left(-\int_{t_0}^{t_1} A(t)+B(t)\ dt\right)\exp\left(-\int_{t_1}^{t} A(t)+B(t)\ dt\right) \tag{B.0.9}$$

$$= \hat{\Delta}(t_0,t) \tag{B.0.10}$$

so that it pull outside the integral to give

$$P_{10} = \hat{\Delta}(t_0,t)A(t) + \hat{\Delta}(t_0,t)A(t)\int_{t_0}^{t} \mathrm{d}t_1 B(t_1) \tag{B.0.11}$$

As a final case before generalization consider where there are two rejected trials before acceptance. The probability of accepting t with either 0, 1, or 2 rejections is

$$P_{210} = P_{10} + \int_{t_0}^{t}\mathrm{d}t_1\int_{t_1}^{t}\mathrm{d}t_2\ \hat{\Delta}(t_0,t_1)B(t_1)\hat{\Delta}(t_0,t_2)B(t_2)\hat{\Delta}(t_1,t)\hat{\Delta}(t_2,t)A(t) \tag{B.0.12}$$

$$= P_{10} + A(t)\left(\hat{\Delta}(t_0,t)\right)^2\int_{t_0}^{t}\mathrm{d}t_1 B(t_1)\int_{t_1}^{t}\mathrm{d}t_2\ B(t_2) \tag{B.0.13}$$

We now notice that

$$\int_{t_0}^{t}\mathrm{d}t_1 B(t_1)\int_{t_1}^{t}\mathrm{d}t_2\ B(t_2) = \int_{t}^{t_0}\mathrm{d}t_1 B(t_1)\int_{t}^{t_1}\mathrm{d}t_2 B(t_2) \tag{B.0.14}$$

and as noted in Fig. 4.1 in Peskin & Schroeder [39] the latter integral is simply half the area of a cube, so we rewrite and observe that

$$\int_{t}^{t_0}\mathrm{d}t_1 B(t_1)\int_{t}^{t_1}\mathrm{d}t_2 B(t_2) = \frac{1}{2}\left(\int_{t_0}^{t} B(t_1)\ \mathrm{d}t_1\right)^2 \tag{B.0.15}$$

So that, using the expression for P_{10} now

$$P_{210} = \hat{\Delta}(t_0,t)A(t)\left[1+\int_{t_0}^{t} B(t_1)\ \mathrm{d}t_1 + \frac{1}{2}\left(\int_{t_0}^{t} B(t_1)\ \mathrm{d}t_1\right)^2\right] \tag{B.0.16}$$

Finally we generalize to the case of n rejected trials to construct the probability of acceptance at t after any number of rejected trials. We will have a nested integral $\int_{t_0}^{t} dt_1 \int_{t_0}^{t_1} dt_2 \int_{t_0}^{t_2} dt_3 \int ... \int_{t_0}^{t_{n-1}} dt_n$ which will in an analogous manner to the above reduce to a fractional volume of the ordered slice $t_0 > t_1 > ... > t_n$ of the n-hypercube with a factor of $1/n!$, so that

$$P(t) = \hat{\Delta}(t_0,t)A(t)\left[1+\sum_{n=1}^{\infty}\frac{1}{n!}\left(\int_{t_0}^{t} B(t_1)\ \mathrm{d}t_1\right)^n\right] \tag{B.0.17}$$

$$\implies P(t) = \hat{\Delta}(t_0,t)A(t)\exp\left(\int_{t_0}^{t} B(t_1)\ \mathrm{d}t_1\right) \tag{B.0.18}$$

$$= A(t)\exp\left(-\int_{t_0}^{t} A(t_1)\mathrm{d}t_1\right) \tag{B.0.19}$$

which is none other than the probability to generate an event at time t following a period of no-evolution from t_0 to t defined by the original Sudakov factor.

We conclude that the veto algorithm exactly reproduces the distribution of branching times t, so that for a suitable function B, a large amount of computational expense can be bypassed. It is the opinion of the author that this is a singularly beautiful result.

Appendix C

Feynman Rules

First we derive the vertex factor for $\phi_i \rightarrow \bar{\psi}_i + \psi$. This should, strictly speaking, be written $\phi_i \rightarrow \bar{\psi}_j + \psi$ and the vertex factor should contain a δ_{ij} to ensure colour conservation, matching to the Lagrangian we have written, and it should contain the usual coupling factor of ig. Now, consider this in analogy to the quark-gluon-quark vertex of QCD. The Lorentz structure for such a process is defined through a fermion-vector-fermion vertex which contains a factor of $ig_s\gamma^\mu t^a_{ij}$, for a gluon with adjoint index a and incoming (outgoing) quarks of colours i (j). Breaking this down we see that the factor of i comes from the perturbative series of the amplitude, the g_s comes from the colour coupling, the colour flow is captured by t^a_{ij} and the vector nature of the vertex is captured by γ^μ, which also reflects the coupling of the gluons to spin-1/2 fermions. In our process we have a fermion-scalar-fermion vertex and thus by analogy, we have a vertex factor of $ig\delta_{ij}$. Whether this vertex is then connected to external or internal lines is taken care of by the rules in [39].

Next we consider the emission of a gluon from a scalar particle as below. Since the gluon line carries a vector we therefore require a vector vertex.

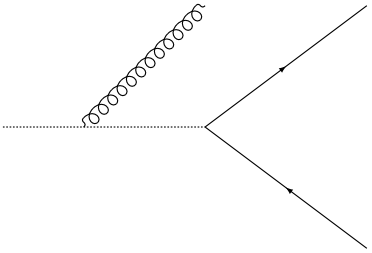

We expect a factor of i as usual, a factor of g_s for the strong coupling, and a vector characterising the vertex. The only vectors which we may use here are the momenta of the scalar particles, since there is no γ^μ in the coupling of ϕ_i to A^μ_a. The amplitude must of course depend on both the incoming and outgoing momenta of the scalar particles. Furthermore the only possible way these momenta may be combined is by addition or subraction, since a multiplication like $k_\mu k'_\nu$ for incoming momentum k and outgoing momentum k' would form a tensor vertex. Therefore the only two possibilities are $(k+k')^\mu$ and $(k-k')^\mu$ and we may see from this fact alone that the vertex factor must include a $(k+k')^\mu$.
The reason for this is that the emitted gluon, bshower iseing an external line to the Feynman diagram, carries a polarization vector $\epsilon^*_\mu(k-k')$ (where * denotes a complex conjugate). Therefore if we choose $(k-k')^\mu$ as the vertex factor, the resultant amplitude carries a factor $(k-k')^\mu\ \epsilon^*_\mu(k-k')$. We work in the Lorenz gauge where boson polarization vectors satisfy $p.\epsilon(p) = 0$, and therefore we

conclude that any vertices containing $(k-k')^\mu$ do not exist. We conclude that the amplitude can contain none other than $ig_s(k+k')^\mu$. Finally we recall that the gluon necessarily alters the colour flow, so there must be a t^a_{ij} factor here as well. We may double check this answer by considering instead the theory of scalar electrodynamics whose vertices are well known. The only difference here is that, as mentioned, the emission of a non-Abelian gauge boson will impact the colour flow and therefore our answer for the chromodynamic process should have an extra t^a_{ij} factor relative to the electrodynamic one. The latter vertex [47] is precisely $ig'(k+k')^\mu$ for some coupling g', from which we conclude that our vertex factor is indeed $ig_s t^a_{ij}(k+k')^\mu$.

We summarize here the Feynman rules which we have used, [23, 39]:

1. External fermions with momentum p, spin s, (colour i) in the final state carry a factor of $\bar{u}^s_{(i)}(p)$, while those in the initial state carry a factor of $u^s_{(i)}(p)$
2. External antifermions in the initial state carry a $\bar{v}^s_{(i)}(p)$ and those in the final state carry a $v^s_{(i)}(p)$
3. External gluons of momentum p in the final state carry a $\epsilon^*_\mu(p)$. They also carry a 'polarization' in the gauge group space, however this will be captured by the t_{ij} matrices and therefore an adjoint index on the ϵ is omitted for clarity.
4. External scalar particles carry a factor of 1
5. Spin-0 propagators of momentum q and mass m carry a factor of $\dfrac{i}{q^2-m^2}$
6. Spin-1/2 propagators of momentum q and mass m carry a factor of $\dfrac{i(\not{q}+m)}{q^2-m^2}$
7. Quark-gluon-quark vertex factor is $ig_s\gamma^\mu$
8. Scalar-gluon-scalar vertex factor is $it^a_{ij}(k+k')^\mu$ for incoming scalar of momentum k and colour i, and outgoing scalar of momentum k' and colour j.
9. Scalar-quark-fermion vertex factor is $i\delta_{ij}g_s$

We finally note that we are free to evalute these amplitudes in a basis where the spins are quantized in the direction of motion of the particles, i.e. the indices s on our spinors u^s, v^s are helicity indices.

Appendix D

Backward radiation for massive b-quark

Using the massive form of Eqs. (3.8.11)-(3.8.13) it is straightforward to compute

$$s_{AK}a^{\mathrm{RF}}_{g/q\tilde{q}} = \frac{m_a E_k}{m_k^2} - \frac{m_a\sqrt{E_k^2 - m_k^2}}{m_k^2} + \frac{\sqrt{E_k^2 - m_k^2}}{E_j} - \frac{E_k}{E_j} - 2 \tag{D.0.1}$$

However, since we have shown the properties of the massive antenna graphically, we will not study this equation analytically.

Appendix E

Solving kinematics for standalone antenna plots

We require the energy of the b quark in the rest frame of a, in terms of the gluon energy and the masses of the other particles, or put differently, we require E_k in terms of E_j, m_a, m_k, m_X. Starting with conservation of 4-momentum, we write

$$p_X = p_a - p_j - p_k \tag{E.0.1}$$

$$\implies m_X^2 = p_a^2 + p_j^2 + p_k^2 - 2p_a.p_j - 2p_a.p_k + 2p_j.p_k \tag{E.0.2}$$

$$m_X^2 = m_a^2 + m_k^2 - 2m_aE_j - 2m_aE_k + 2E_j(E_k - \sqrt{E_k^2 - m_k^2}\cos(\theta_{jk})) \tag{E.0.3}$$

Solving this as a quadratic in E_k gives two solutions:

$$E_k^+ = \frac{-E_j\left(3m_a^2 + m_k^2 - m_X^2 - \sqrt{\Delta}\right) + 2m_aE_j^2 + m_a\left(m_a^2 + m_k^2 - m_X^2\right)}{2\left(-2m_aE_j + m_a^2 + E_j^2\sin^2\left(\theta_{\mathrm{jk}}\right)\right)} \tag{E.0.4}$$

$$E_k^- = \frac{-E_j\left(3m_a^2 + m_k^2 - m_X^2 + \sqrt{\Delta}\right) + 2m_aE_j^2 + m_a\left(m_a^2 + m_k^2 - m_X^2\right)}{2\left(-2m_aE_j + m_a^2 + E_j^2\sin^2\left(\theta_{\mathrm{jk}}\right)\right)} \tag{E.0.5}$$

where, so that the equations can fit on one line, we have defined

$$\begin{aligned}\Delta = &\cos^2\left(\theta_{\mathrm{jk}}\right)\\ &\times \quad \Big[4E_j^2\left(m_a^2 - m_k^2\sin^2\left(\theta_{\mathrm{jk}}\right)\right) + 4m_aE_j\left(-m_a^2 + m_k^2 + m_X^2\right)\\ &+ \quad -2m_X^2\left(m_a^2 + m_k^2\right) + \left(m_a^2 - m_k^2\right)^2 + m_X^4\Big]\end{aligned}$$

Deciding which solution to take is a nontrivial matter even after plotting the results, since both are positive.

To constrain the solution we will study the limiting case when the gluon is emitted exactly collinear to the b particle, so that $\theta_{jk} = 0$, and for further simplicity we will take $m_b = 0$ (the kinematical relations will still hold). In the rest frame of a

$$\vec{p}_X = -\vec{p}_j - \vec{p}_k \tag{E.0.6}$$

So squaring and using the mass shell conditions,

$$E_X^2 - m_X^2 = \vec{p}_j^{\,2} + 2\vec{p}_j.\vec{p}_k + \vec{p}_k^{\,2} \tag{E.0.7}$$

$$E_X^2 = m_X^2 + E_j^2 + 2|\vec{p}_j||\vec{p}_k|\cos(0) + E_k^2 \tag{E.0.8}$$

$$\therefore\ E_X^2 = m_X^2 + E_j^2 + 2E_jE_k + E_k^2 \tag{E.0.9}$$

Then using $p_X = p_a - p_j - p_k$, energy conservation gives $E_X = m_a - E_j - E_k$ so that

$$(m_a - E_j - E_k)^2 = m_X^2 + E_j^2 + 2E_jE_k + E_k^2 \tag{E.0.10}$$

Solving this again for E_k we find

$$E_k = \frac{1}{2}\left(-2E_j + m_a - \frac{m_X^2}{m_a}\right) \tag{E.0.11}$$

Using $m_a = 175, m_X = 80.3$, and for illustration using high energy $E_j = 10^{1.8}$ GeV where the difference is large, we obtain $E_k = 5.98115$ GeV while our two solutions give $E_k^+ = 21.4451$ GeV and $E_k^- = 5.98115$ GeV. Thus we have that E_k^- is correct.

Appendix F

Lie Groups

We will here make some brief comments on Lie group theory, in a lightning paced review of the first two chapters of [48].

The definition of a Lie group is a group whereby each element of the group is related to the identity element continuously. For instance in $U(1)$ the element $e^{i\alpha}$ is related to the identity e^{i0} by successive applications of an infinitesimal $U(1)$ transformation. Namely, beginning with the identity I we take some infinitesimal displacement $I + A$. At this stage we will note that this holds for any n-dimensional $U(n)$ group and the discussion is independent of n.
The infinitesimal displacement may be defined by the group property of $U(n)$ such that $(I+A)(I+A)^\dagger = I$, i.e. $I + A$ is still a unitary matrix. Expanding, we have $I + IA^\dagger + AI = I$, noting that as A is infinitesimal, $AA^\dagger$ can be neglected. This yields the condition $A = -A^\dagger$, and suggests that any infinitesimal displacement matrix must be an antihermitian matrix. Thus we construct a basis of antihermitian matrices, which may easily be done in any dimension but as the discussion is irrelevant we will here omit it. These basis matrices are known as generators. In general we have that $A = \sum \theta_i \mathcal{J}_i$ where $\mathcal{J}_i$ is the i^{th} of n generators in an n-dimensional group, and θ_i is the displacement in the i^{th} direction. For different groups, the condition on the infinitesimal displacements may be different, for instance one may find that they must be orthogonal rather than antihermitian. Let us say that infinitesimal displacements must satisfy some condition X. In each case, one may construct a basis for matrices of condition X.
With this, we may define for instance a $U(1)$ transformation; which is none other than a rotation; of finite angle θ by iterating N successive applications of an infinitesimal angular displacement $R(\Delta\theta) = 1 + A = 1 + \Delta\theta\mathcal{J} = 1 + \frac{\theta\mathcal{J}}{N}$ and taking the limit as $N \to \infty$. We have the θ^{th} group element of $U(1)$,

$$x(\theta) = \lim_{N\to\infty} \left(I + \frac{\theta\mathcal{J}}{N}\right)^N =: e^{\theta\mathcal{J}} \tag{F.0.1}$$

It is typically a matter of convention how one defines the generators; they are non unique, and are defined such that they satisfy the Lie Algebra of the group, which is unique. In particular this means that any generators of a group must satisfy $[A, B] = f_G$ where f_G is some arbitrary expression depending on the group G. In fact one may write, for a set of generators $\{A_i\}$ of a group, the Lie Algebra $[A_i, A_j] = if_{ijk}A^k$. The functions f_{ijk} are known as structure constants and a specification of these uniquely defines the group. Different representations of the group are obtained by finding different matrices (or any objects) which satisfy the Lie Algebra. We will say no more on Lie Algebras here.
Given this, it is advantageous to redefine generators such that $x(\theta) = e^{i\theta J}$ rather than $e^{\theta\mathcal{J}}$. This

modifies the condition on the generators slightly. For $U(1)$ we may trivially see that the only generator is $\mathcal{J} = i$, since $i^\dagger = -i$. This suggests $J = 1$, and leaves us with the $U(1)$ rotation element of angle θ as $x(\theta) = e^{i\theta}$. Finally, if we wish to specialize to the special unitary group $SU(n)$ for $n > 1$, we simply enforce that the determinant of any group element, if represented as a matrix, is one.

Returning to gauge transformations, we see this $U(1)$ element $x(\theta)$ may act as a global gauge transformation on the field. We may easily map $e^{i\theta}$ to some $e^{i\lambda(x)}$ within the group structure, for an arbitrary $\lambda : \mathbb{R}^{N+1} \to \mathbb{R}$ for $N+1$ spacetime dimensions. This is now a local gauge transformation, and is precisely the gauge symmetry of QED.

References

[1] G. Hanson et al. Evidence for Jet Structure in Hadron Production by e^+e^- Annihilation. *Phys. Rev. Lett.*, 35:1609–1612, Dec 1975.

[2] G. Hanson et al. Hadron production by e^+e^- annihilation at center-of-mass energies between 2.6 and 7.8 GeV. II. Jet structure and related inclusive distributions. *Phys. Rev. D*, 26:991–1012, Sep 1982.

[3] Adye, Tim. First W+ W- Event Observed At LEP. URL: `http://hepunx.rl.ac.uk/~adye/4j.html`, 1996/2007.

[4] B Vachon. W+ W- Production at the Large Electron Positron Collider. *University of Victoria, Candidacy Paper*, 1999.

[5] E Norrbin and Torbjörn Sjöstrand. QCD radiation off heavy particles. *Nuclear Physics B*, 603 (1-2):297–342, 2001.

[6] Bryan R Webber. Monte Carlo simulation of hard hadronic processes. *Annual Review of Nuclear and Particle Science*, 36(1):253–286, 1986.

[7] Jessie Shelton. TASI lectures on jet substructure. *arXiv preprint arXiv:1302.0260*, 2013.

[8] James D Bjorken and Emmanuel A Paschos. Inelastic electron-proton and γ-proton scattering and the structure of the nucleon. *Physical Review*, 185(5):1975, 1969.

[9] Richard P Feynman. Very high-energy collisions of hadrons. *Physical Review Letters*, 23(24): 1415, 1969.

[10] Yuri L Dokshitzer. Calculation of the structure functions for deep inelastic scattering and e^+e^- annihilation by perturbation theory in quantum chromodynamics. *Zh. Eksp. Teor. Fiz*, 73:1216, 1977.

[11] Vladimir Naumovich Gribov and Lev N Lipatov. Deep inelastic *ep*-scattering in a perturbation theory. Technical report, Inst. of Nuclear Physics, Leningrad, 1972.

[12] LN Lipatov. The parton model and perturbation theory. *Sov. J. Nucl. Phys.*, 20:94–102, 1974.

[13] Guido Altarelli and Giorgio Parisi. Asymptotic freedom in parton language. *Nuclear Physics B*, 126(2):298–318, 1977.

[14] Andy Buckley, Jonathan Butterworth, Stefan Gieseke, David Grellscheid, Stefan Höche, Hendrik Hoeth, Frank Krauss, Leif Lönnblad, Emily Nurse, Peter Richardson, et al. General-purpose event generators for LHC physics. *Physics Reports*, 504(5):145–233, 2011.

[15] Peter Skands. Introduction to QCD. In *Searching for New Physics at Small and Large Scales: TASI 2012*, pages 341–420. World Scientific, 2013.

[16] Nadine Fischer, Stefan Prestel, Mathias Ritzmann, and Peter Skands. Vincia for hadron colliders. *The European Physical Journal C*, 76(11):589, 2016.

[17] Gösta Gustafson and Ulf Pettersson. Dipole formulation of QCD cascades. *Nuclear Physics B*, 306(4):746–758, 1988.

[18] Gösta Gustafson. Dual description of a confined colour field. *Physics Letters B*, 175(4):453–456, 1986.

[19] Ya I Azimov, Yu L Dokshitzer, Valery A Khoze, and SI Troyan. The string effect and QCD coherence. *Physics Letters B*, 165(1-3):147–150, 1985.

[20] David Tong. Lectures on quantum field theory. *Part III Cambridge University Mathematics Tripos, Michaelmas*, 2006.

[21] R Keith Ellis, W James Stirling, and Bryan R Webber. *QCD and collider physics*. Cambridge university press, 2003.

[22] David J Gross and Frank Wilczek. Ultraviolet behavior of non-abelian gauge theories. *Physical Review Letters*, 30(26):1343, 1973.

[23] David Griffiths. *Introduction to elementary particles*. John Wiley & Sons, 2008.

[24] Francis Halzen and Alan D Martin. *Quark & Leptons: An Introductory Course In Modern Particle Physics*. John Wiley & Sons, 2008.

[25] AM Sirunyan et al. Study of the underlying event in top quark pair production in *pp* collisions at 13 TeV. *The European Physical Journal. C, Particles and Fields*, 79(2), 2019.

[26] M. Aaboud et al. Measurements of higgs boson properties in the diphoton decay channel with 36 fb^{-1} of *pp* collision data at $\sqrt{s} = 13$ TeV with the ATLAS detector. *Physical Review D*, 98 (5):052005, 2018.

[27] ALICE Collaboration. Underlying Event properties in pp collisions at $\sqrt{s} = 13$ TeV, 2019.

[28] Toichiro Kinoshita. Mass singularities of Feynman amplitudes. *Journal of Mathematical Physics*, 3(4):650–677, 1962.

[29] Tsung-Dao Lee and Michael Nauenberg. Degenerate systems and mass singularities. *Physical Review*, 133(6B):B1549, 1964.

[30] A Kadeer and JG Korner. Radiative corrections to top quark decays. *arXiv preprint arXiv:0906.3474*, 2009.

[31] Massimiliano Grazzini, Stefan Kallweit, Dirk Rathlev, and Marius Wiesemann. W±Z production at hadron colliders in NNLO QCD. *Physics Letters B*, 761:179–183, 2016.

[32] Torbjörn Sjöstrand, Stephen Mrenna, and Peter Skands. PYTHIA 6.4 physics and manual. *Journal of High Energy Physics*, 2006(05):026, 2006.

[33] Aude Gehrmann-De Ridder, Mathias Ritzmann, and Peter Skands. Timelike dipole-antenna showers with massive fermions. *Physical Review D*, 85(1):014013, 2012.

[34] S Mrenna and P Skands. Automated parton-shower variations in Pythia 8. *Physical Review D*, 94(7):074005, 2016.

[35] Torbjörn Sjöstrand and Peter Z Skands. Transverse-momentum-ordered showers and interleaved multiple interactions. *The European Physical Journal C-Particles and Fields*, 39(2): 129–154, 2005.

[36] F Abe et al. Evidence for color coherence in pp collisions at $\sqrt{s} = 1.8$ TeV. *Physical Review D*, 50(9):5562, 1994.

[37] Keith Hamilton and Peter Richardson. A simulation of QCD radiation in top quark decays. *Journal of High Energy Physics*, 2007(02):069, 2007.

[38] Helen Brooks and Peter Skands. Coherent showers in decays of colored resonances. *Phys. Rev. D*, 100:076006, Oct 2019. doi: 10.1103/PhysRevD.100.076006. URL `https://link.aps.org/doi/10.1103/PhysRevD.100.076006`.

[39] Michael E Peskin. *An introduction to quantum field theory*. CRC Press, 2018.

[40] Masaharu Tanabashi et al. Review of Particle Physics. *Physical Review D*, 98(3):030001, 2018.

[41] Walter T Giele, David A Kosower, and Peter Z Skands. A simple shower and matching algorithm. *Physical Review D*, 78(1):014026, 2008.

[42] A Gehrmann-De Ridder and M Ritzmann. NLO antenna subtraction with massive fermions. *Journal of High Energy Physics*, 2009(07):041, 2009.

[43] Sun-Sheng Shei and Hung-Sheng Tsao. Scalar quantum chromodynamics in two dimensions and the parton model. *Nuclear Physics B*, 141(4):445–466, 1978.

[44] Alexander Belyaev, Neil D Christensen, and Alexander Pukhov. CalcHEP 3.4 for collider physics within and beyond the Standard Model. *Computer Physics Communications*, 184(7): 1729–1769, 2013.

[45] Yu L Dokshitzer, Valery A Khoze, and SI Troyan. On specific QCD properties of heavy quark fragmentation ('dead cone'). *Journal of Physics G: Nuclear and Particle Physics*, 17(10):1602, 1991.

[46] Fabio Maltoni, Michele Selvaggi, and Jesse Thaler. Exposing the dead cone effect with jet substructure techniques. *Physical Review D*, 94(5):054015, 2016.

[47] Daniele Binosi and Joannis Papavassiliou. Pinch technique for Schwinger-Dyson equations. *Journal of High Energy Physics*, 2007(03):041, 2007.

[48] Anthony Zee. *Group theory in a nutshell for physicists*, volume 17. Princeton University Press, 2016.